CDF/ANAL/EXOTIC/CDFR/10096
Version 1.0
October 11, 2011

Likelihood-Based Lepton Identification to Search for the Vh Production

Toru Okusawa, Yoshihiro Seiya, Takayuki Wakisaka,
Kazuhiro Yamamoto, Daisuke Yamato, and Mina Yoshida

Osaka City University, Japan

Abstract

We search for the neutral higgs production associated with the weak vector-boson using hight-p_T like-sign (LS) dilepton events. It is important to distinguish real and fake leptons in this search because fake leptons are one of major backgrounds in the LS dilepton events. At CDF, we usually use cut-based identification (ID) methods for the lepton selection in high-p_T regions, but given that higgs searches are difficult mainly due to small predicted production cross sections, it is worth to consider more sophisticated lepton selections. This note describes the lepton ID using a likelihood method for electrons and muons. The method combines the probability distribution functions (PDFs) of various lepton ID variables into a single likelihood function. We compare efficiencies of the likelihood-based ID with those of the cut-based ID using signal and background samples to estimate improvements. We look at 3 types of signal control samples: Z decays, photon conversions (for electrons), and higgs Monte Carlo (MC) samples, while the background (fake lepton) control samples are inclusive jet data. For the same efficiencies of leptons from Z decays as the cut-based ID, the signal-to-background ratios are found to be improved by factors of 3.6–9.1 for electrons and 1.3–1.8 for muons, depending on the p_T, using the signal PDFs created from Z decays themselves. Using the same PDFs, the efficiency for electrons is increased by a factor of about 1.3, while it is about 1.1 for muons, for the same fake-lepton efficiencies. Our likelihood-based ID is confirmed to be better than the cut-based method for leptons, especially for electrons, from Z decays. For the selection of electrons in higgs MC events, the PDFs created from higgs MCs showed slightly better performance than the PDFs by Z events, while we did not see significant improvements for the muon selection.

1 Introduction

Our physics objective is to search for the neutral higgs boson using like-sign (LS) dilepton events produced by the process

$$qq' \to Vh \to V(W^*W^*) \to \ell^\pm\ell^\pm + X\ , \qquad V = W,\ Z\ . \tag{1}$$

The relevant higgs boson mass region is above 160 GeV/c^2 for the Standard Model (SM) higgs boson where the branching fraction of $H \to WW^*$ supersedes that of $H \to b\bar{b}$. However, the search for this signature in low-mass regions is also important because we need to investigate various higgs boson couplings to confirm that they are consistent with what we expect from the SM. This channel also covers the case beyond the SM where the higgs boson couples only to the gauge bosons, which is referred to as the fermiophobic higgs boson. On the experimental side, the LS dilepton event is one of the cleanest signature in hadron collisions. This analysis is therefore expected to have a high potential for the higgs boson search.

The LS requirement is quite effective to suppress QCD and known electroweak processes, however fake-lepton backgrounds still remain at a considerable level. We traditionally use cut-based identification (ID) methods for the lepton selection in high-p_T physics analyses, but given that the higgs search is difficult mainly due to small predicted production cross-sections, developments of more sophisticated ID methods are worth to pursue. In this note, we investigate a likelihood-based lepton ID (LLID) which combines various lepton ID variables into a single likelihood function and compare efficiencies with those of our cut-based ID method (CLID) which is fairly standard.

2 Likelihood function

The likelihood-based lepton identification itself is not new at CDF but can be found in applications to low-p_T regions [1]. With control samples of real and fake leptons, we separately normalize distributions of ID variables, taking into account of the bin widths of histograms[1], to obtain the probability distribution functions (PDFs). We define the likelihood that a lepton candidate is indeed a real lepton to be

$$S = \prod_{i=1}^{n} S_i\ , \tag{2}$$

ignoring any correlations between the ID variables, where S_i is the PDF of real leptons for the i-th ID variable. The likelihood that the lepton candidate is a fake lepton is similarly given as

$$B = \prod_{i=1}^{n} B_i\ . \tag{3}$$

[1] As long as we use the same binning for a given variable between the signal and background, which we actually do, the bin width cancels out in the final likelihood estimator.

The final likelihood estimator is constructed by

$$L = \frac{S}{S+B} \,. \tag{4}$$

We expect that lepton candidates with values of L close to unity are real leptons, while values close to zero indicate most probably fake leptons.

3 Lepton identification variables

3.1 Electron

The basic identification variables used to calculate the likelihood for electron selection are mostly obtained by using the `ElectronUser/StdCEMElectron` class. We choose 8 variables for our likelihood method.

- E/p
  This is defined by the ratio of the cluster energy to the beam-constrained COT-track momentum. To clarify, we comment that the E/p in the electron selection is not E_T/p_T. If the object is an electron, its momentum measured by the COT track should match with the energy measured for the calorimeter cluster, i.e. $E/p \simeq 1$.

- $\chi^2_{\rm strip}$
  The pulse height shape in the strip view (r-z) of the CES detector is compared to the same profile extracted from test-beam data of electrons using χ^2 test. The $\chi^2_{\rm strip}$ is scaled up using a global function `scaleCesChisq` to correct for energy dependence[2].

- HA/EM
  This quantity is the ratio of 2-tower hadronic energy deposited in the CHA/WHA to the 2-tower electromagnetic energy deposited in the CEM. This ratio should be small, that is, the energy deposition in the electromagnetic calorimeter is much higher than that in the hadronic calorimeter.

- $L_{\rm shr}$
  The purpose of this quantity is to provide some discrimination of electrons and photons from hadronic showers faking these particles in the CEM. This is done by comparing the observed energy sharing between towers to that expected for a true electromagnetic shower taken from test-beam data:

$$L_{\rm shr} = 0.14 \sum_i \frac{E_i^{\rm adj} - E_i^{\rm exp}}{\sqrt{(0.14\sqrt{E})^2 + (\Delta E_i^{\rm exp})^2}} \,, \tag{5}$$

[2]Basically, it attempts to multiply $\sqrt{E}$.

where E_i^{adj} is the measured energy in towers adjacent to the seed tower, E_i^{exp} is the expected energy in the adjacent towers from test beam data, $\Delta E_i^{\mathrm{exp}}$ is the error on the energy estimate.

- $Q \times \Delta x_{\mathrm{CES}}$
  The Δx_{CES} is the distance, in units of cm, in the r-ϕ plane between the track extrapolated to the radius of the CES and the actual cluster position measured by the CES. We sign it with the charge of the candidate track.

- Δz_{CES}
  This variable is the distance, in units of cm, in the r-z plane between the track extrapolated to the CES radius and the actual cluster position measured by the CES.

- E_{CES}/p^*
  This is the ratio of the wire cluster pulse height measured in the CES, corrected for chamber warps, to the $p^* = 10(p/10)^{\alpha}$, where the p is the track momentum and α is defined in Eq. (**??**). The value for a real electron is expected to be around 1. The CES responses are sensitive to the shower development which is expected to be different between electrons and interactive pions.

- CPR or CP2
  The response of the CPR or CP2 detector corresponding to an EM-calorimeter cluster in units of the number of minimum-ionizing-particles (MIPs). The peak position corresponding to one MIP is identified by using muons. The CPR/CP2 responses are also sensitive to the shower-development as well as the CES responses.

3.2 Muon

We choose 4 and 3 variables to define our likelihood function for CMUP and CMX muons, respectively.

- EM and HA
  Muons deposite small energies in the calorimeters due to the ionization. In order to maintain good efficiencies for high energy muons, the cuts are dependent on the momentum.

- $r \times \Delta\phi$
  This quantity is the track-stub matching in the r-ϕ plane and defined for each of the CMU, CMP, and CMX muon detectors. The matching is dependent on the p_T due to the effects of multiple scattering.

4 Real-lepton samples

4.1 Leptons from Z decays

A natural choice of real-lepton control sample is the leptons from Z decays. The high-p_T inclusive lepton samples, `bhel*` and `bhmu*`, corresponding to an integrated luminosity of 4.8 pb^{-1} are used to select these leptons. We apply the same asymmetric kinematical cuts as our previous higgs search analysis [2], where the high-p_T cut is $E_T > 20$ GeV ($p_T > 10$ GeV/c) for leading electrons or $p_T > 20$ GeV/c for muons, while the low-p_T cut is $E_T > 6$ GeV ($p_T > 6$ GeV/c) for electrons or $p_T > 6$ GeV/c for muons. The leading lepton is required to fully pass other lepton selections using our CLID[3] which is listed in Table 1. The 2nd lepton, which serves as a probe, is required to pass the track quality and isolation cuts. The conversion veto is also applied if it is an electron candidate. In order to ensure leptons be originating from Z decays, we require the two leptons have opposite charges and the invariant mass in a Z-mass window 81–101 GeV/c^2.

Figures 1 and 2 show E_T and p_T distributions of probe leptons from Z decays. Although the kinematical cut on the probe leptons is $p_T > 6$ GeV/c, the leptons from Z decays have much higher typical p_T because of the heavy mass of the Z boson. The distributions from the higgs Monte Carlo (MC) samples for the mass of 110 GeV/c^2 and 160 GeV/c^2 are also included in the figures. As we see, the leptons from the higgs boson do not necessarily have such high p_T as Z leptons. Since the lepton ID variables have energy dependences in general[4], mismatches of the p_T region between the sample used to construct the PDFs and that the LLID is applied to would introduce inefficiencies.

4.2 Electrons from photon conversions

As an attempt to create PDFs covering relatively low-p_T electrons, we collect conversion electrons with the same 6 GeV/c cut in the high-p_T inclusive electron samples. The E_T and p_T distributions are already shown in Fig. 1. We have more electrons in lower p_T regions compared to the Z electrons but the situation that there are mismatches in the p_T regions is basically the same. Because of requiring the presence of a high-p_T electron besides a photon-conversion to ensure the triggering, these events are basically dielectron events and seem to be coming from $Z \rightarrow ee$ events. We might have to use high-p_T muon samples or low-p_T inclusive lepton samples if we want to pursue this direction of the analysis, which we do not include in this note.

[3] The $r \times \Delta\phi$ cut for CMUP muons is a logical "and" of each CMU and CMP matching as in the standard cut. We comment that the CMU matching of 3 cm is out of date in the standard cut.

[4] For example, HA/EM or CPR responses.

4.3 Leptons from higgs Monte Carlo samples

What happens if we directly use higgs MCs to create signal PDFs to ensure p_T-region matching? This is probably a new idea at CDF. We usually use signal MCs to contruct final discriminants based on various kinematical/topological information to separate signals from backgrounds in the final samples, but usually do not for the event selection at lower levels such as the lepton ID. Immediate issues are, of course, possible mis-modeling of the ID variables by the MCs. They particularly result in over-efficiencies for the higgs MC-events compared to real higgs-events that might exist in the data. But one can see that the issues are not special to this scheme. We have to deal with any aspects of mis-modeling by the MCs anyways no matter what kind of event selection we perform, and we argue that the situation is the same as the usual CLID case. Effects of mis-modeling are, then, to be absorbed in the relevant, the so-called, scale factors. Final checks can be done by measuring cross-section of known physics processes, and comparing background expectations with the data in control and/or pilot regions with various kinematical biases. It is we think interesting to see if this scheme improves the identification performance. We note, however, that we would not introduce higgs-based PDFs unless the improvements are significant because the model-dependences at low levels of analyses introduce practical difficulties such as repeating a large potion of the analysis everytime the base information is altered.

5 Fake-lepton samples

The words "fake leptons" here are used to mean rather generic objects including non-prompt real leptons such as those coming from (semi-)leptonic decays of heavy-flavor hadrons as well as literal fake leptons. The same selection as is used for the probe leptons of the signal samples is applied to generic jet samples and resulting "lepton" candidates are considered to form the fake-lepton control samples. The jet samples are collected with the so-called `Jet20`, `Jet50`, `Jet70`, and `Jet100` triggers, and the corresponding integrated luminosity is 4.8 pb^{-1}. The events from different triggers are combined with the weights reflecting the nominal trigger pre-scales, as shown in Fig. 3.

6 Probability distribution functions

Figures 4–8 compares the signal and background PDFs, where the signal leptons come from Z decays. The effects of mis-modeling the signal distributions by the MCs will be corrected for by scale factors which are obtained by comparing efficiencies between real data and MCs for known processes which are usually Z events. We compare signal PDFs between Z events of the data and MCs in Figs. 9–13. For the E_{CES}/p^* and CPR/CP2 responses of MC data, we find the peak positions are systematically shifted from those found in the real data. We thus apply rescaling factors to the MC responses to match the distributions as much as possible. These factors are 0.754 for the E_{CES}/p^*, 0.557 for the CPR, and 0.506 for the CP2.

We consider not only electrons from Z decays but also conversion electrons as a signal sample. The PDFs from the Z and conversions are compared in Figs. 14–16. Distributions look similar due to the similar p_T regions we are looking at for the two samples.

Figures 17–21 compare the lepton PDFs of the MCs between the Z and higgs events. The differences seen in the figures represent the MC predictions of p_T dependence of the ID variables.

7 Efficiency

7.1 Electron

Figure 22 shows normalized likelihood distributions for signal and background samples using the signal PDFs based on the Z leptons, where the signal samples are Z, higgs MCs for the mass of 110 GeV/c^2, and 160 GeV/c^2.

The CLID efficiencies for electrons in the Z data, higgs MC samples, and fake electrons in jet samples are shown in Table 2. We estimate the efficiency by the following simple fraction:

$$\varepsilon = \frac{\text{the number of events passing the ID cuts}}{\text{the number of events before the ID cuts}}\,. \tag{6}$$

It is therefore the event efficiency rather than the efficiency per lepton. The efficiency for the Z electrons is 0.776, while it is 0.185 for the fake electrons in the `Jet20` sample.

The cut values for the likelihood that give the same CLID background-efficiencies and the corresponding LLID signal-efficiencies are listed in Table 3, where we use the signal PDFs based on the Z leptons. We see about 30% gains for Z electrons with the LLID. The likelihood cut-values giving the same CLID signal-efficiencies and the corresponding LLID background-efficiencies are also included in the table. For example, the fake efficiency is reduced from 0.185 to 0.019 for the `Jet20`, the signal-to-background ratio (S/B) is thus improved by a factor of 9.6. According to the table, the S/B improvement is gradually reduced as the jet trigger E_T becomes higher. Similar analyses for the higgs MCs of the mass 110 GeV/c^2 and 160 GeV/c^2 are also shown in the table. The results for other higgs masses are given in Table 4, while the cases using the signal PDFs based on higgs MCs are listed in Tables 5–6.

Figure 23 compares the signal-efficiency vs. the background-efficiency curves for 3 samples: Z, higgs with the mass 110 GeV/c^2, and 160 GeV/c^2, for a given type of the PDFs, where the background sample is fixed to be the `Jet20`. Figure 24 compares the same curves using the different signal PDFs for a given sample.

We confirm that the LLID is better than the CLID for electrons. The PDFs created from higgs MCs showed slightly (a few %) better performance than using the PDFs from Z data to apply for higgs MCs, although it is not certain that the improvements will remain after including scale factors.

7.2 Muon

The same analysis is performed for muons. The results are shown in Tables 7–16. The improvements by the LLID are moderate compared to the electron case: $\simeq 10\%$ gains in signal efficiencies for the same background levels as the CLID, while a factor of $\simeq 1.5$ reduction of backgrounds for the same signal efficiency as the CLID.

8 Cut optimization

We discussed the LLID performance in the previous section using the CLID efficiencies as the reference. If we consider, however, the limits on the higgs production as a measure of the performance, the conclusions are not necessarily the same.

We compute limits based on counting experiments obtained by the CLID. The limits are mapped on the signal vs. background plane by rescaling the signal and background yields from the CLID analysis with uncertainties fixed to nominal values. On the other hand, we know the efficiency ratios between the LLID and the CLID as a function of cut value for the LLID. We can then cast the LLID performance on the limit maps to connect the LLID efficiencies and the limits on the higgs production. It should, however, be noted that the actual limit calculations include physics backgrounds such as WZ events which are not reduced by the LLID, and also use output distributions from final discriminants[5], not the counting experiment. The improvements discussed here are thus not representing the quantitatively final values.

8.1 Electron

We compare the limits on the higgs production using the signal PDFs based on Z decays, photon conversions, and higgs MCs, as a function of cut value for the likelihood. The limits for the higgs MC of 110 GeV/c^2 and 160 GeV/c^2 are shown in Fig. 25. Figures 26–27 show the limits for all the other higgs-mass points. The PDFs based on the higgs MCs show slightly better performance, a few % levels, than those based on the Z events. Final improvements must be investigated after including the corresponding scale factors because there could be over-efficiencies as a result of constructing PDFs from the signal MCs themselves, and it is not certain that such small improvements will still remain.

8.2 Muon

The limits for muon analysis are shown in Figs. 28–33. We do not see any significant performance improvements for the muon case.

[5]The boosted decision tree in our case [3].

9 Conclusion

We have developed a likelihood-based method for the electron and muon identification by using the normalized distributions of various identification variables as the probability distribution functions to be combined to form a single likelihood function.

We investigated possible choices of the probability distribution functions for real leptons: Z decays, photon conversions for electrons, and higgs Monte Carlo events, while we used lepton candidates in inclusive jet samples as fake leptons. Since photon conversions were extracted from the high-p_T inclusive lepton samples, we did not see any significant differences from the case of using the PDFs based on Z electrons.

The likelihood-based lepton identification was found to be better than the cut-based lepton identification, especially for electrons. The probability distribution functions created from higgs Monte Carlo events showed slightly better performances, a few % levels, for identifying electrons from higgs decays in terms of the limits on the production cross section, although it is not certain that such small-level improvements will remain after including relevant scale factors. For muons on the other hand, we did not see any significant differences of performance between the PDFs based on Z events and higgs Monte Carlos.

Table 1: Event pre-selection and cut-based lepton selection.

Electron selection	Muon selection
Event pre-selection	
$\lvert z_{\text{pv}}\rvert < 60$ cm	
Cosmic-ray veto	
Geometrical and kinematical cuts	
CEM	CMUP or CMX
Fiducial	CMU, P: (x,z)-fid $<$ (0,0), (0,$-$3) cm
	CMX: (x,z)-fid $<$ (0,$-$3) cm, $\rho_{\text{COT}} > 140$ cm
	Blue-beam veto, keystone veto, miniskirt veto
$E_T^{\ell_1} > 20$ GeV ($p_T > 10$ GeV/c)	$p_T^{\ell_1} > 20$ GeV/c
$E_T^{\ell_2} > 6$ GeV ($p_T > 6$ GeV/c)	$p_T^{\ell_2} > 6$ GeV/c
Track quality cuts	
Axial ≥ 3 and stereo ≥ 3 (≥ 7 hits)	
$\lvert z_0 - z_{\text{pv}}\rvert < 2$ cm	
$\lvert d_0\rvert < 0.02$ cm	
Isolation cut	
$\text{ISO}_{0.4}^{\text{cal}} < 2$ GeV	
Identification cuts	
HAD/EM $< 0.055 + 0.00045 \times E$	EM $< \max(2, 2 + 0.0115 \times (p - 100))$ GeV
$L_{\text{shr}} < 0.2$ ($E_T < 70$ GeV)	HAD $< \max(6, 6 + 0.0280 \times (p - 100))$ GeV
$E/p < 2$ ($E_T < 50$ GeV)	$\lvert r \times \Delta\phi\rvert < 3, 5, 6$ cm (CMU, P, X)
$\chi^2_{\text{strip}} < 10$	
$\lvert\Delta z_{\text{CES}}\rvert < 3$ cm	
$-3.0 < Q \times \Delta x_{\text{CES}} < 1.5$ cm	
Other cuts	
Conversion removal	

Table 2: Efficiencies of the cut-based method for electron selection.

Sample	total	pass	efficiency
EL	59368	46057	0.776 ± 0.002
Wh110	14689	11441	0.779 ± 0.003
Wh120	15619	11777	0.754 ± 0.003
Wh130	16637	12429	0.747 ± 0.003
Wh140	17843	13281	0.744 ± 0.003
Wh150	18494	13653	0.738 ± 0.003
Wh160	18223	13236	0.726 ± 0.003
Wh170	18693	13567	0.726 ± 0.003
Wh180	19672	14435	0.734 ± 0.003
Wh190	20564	15073	0.733 ± 0.003
Wh200	21011	15341	0.730 ± 0.003
JT20	58933	10880	0.185 ± 0.002
JT50	21821	3563	0.163 ± 0.003
JT70	28838	5195	0.180 ± 0.002
JT100	28338	5565	0.196 ± 0.002

Table 3: Efficiencies of the likelihood-based method for electron selection compared to the cut-based method at the same background efficiencies or the same signal efficiencies. The signal PDFs are created from Z events.

Sample	Same background efficiency			Same signal efficiency		
	L cut	new el efficiency	improvement	L cut	new jt efficiency	reduction
JT20	0.04	0.987 ± 0.000	× 1.3	0.99	0.019 ± 0.001	× 9.6
JT50	0.16	0.979 ± 0.001	× 1.3	0.99	0.029 ± 0.001	× 5.5
JT70	0.17	0.978 ± 0.001	× 1.3	0.99	0.039 ± 0.001	× 4.6
JT100	0.19	0.977 ± 0.001	× 1.3	0.99	0.052 ± 0.001	× 3.8
	L cut	new wh110 efficiency	improvement	L cut	new jt efficiency	reduction
JT20	0.04	0.892 ± 0.003	× 1.1	0.76	0.074 ± 0.001	× 2.5
JT50	0.16	0.873 ± 0.003	× 1.1	0.76	0.091 ± 0.002	× 1.8
JT70	0.17	0.872 ± 0.003	× 1.1	0.76	0.108 ± 0.002	× 1.7
JT100	0.19	0.870 ± 0.003	× 1.1	0.76	0.127 ± 0.002	× 1.5
	L cut	new wh160 efficiency	improvement	L cut	new jt efficiency	reduction
JT20	0.04	0.866 ± 0.003	× 1.2	0.93	0.045 ± 0.001	× 4.1
JT50	0.16	0.855 ± 0.003	× 1.2	0.93	0.062 ± 0.002	× 2.6
JT70	0.17	0.854 ± 0.003	× 1.2	0.93	0.076 ± 0.002	× 2.4
JT100	0.19	0.852 ± 0.003	× 1.2	0.93	0.093 ± 0.002	× 2.1

Table 4: Efficiencies of the likelihood-based method for electron selection compared to the cut-based method at the same background efficiencies or the same signal efficiencies. The samples are higgs MC events of masses other than 110 GeV/c^2 and 160 GeV/c^2. The signal PDFs are created from Z events.

Sample	Same background efficiency			Same signal efficiency		
	L cut	new wh120 efficiency	improvement	L cut	new jt efficiency	reduction
JT20	0.04	0.885 ± 0.003	× 1.2	0.83	0.065 ± 0.001	× 2.8
JT50	0.16	0.867 ± 0.003	× 1.2	0.83	0.081 ± 0.002	× 2.0
JT70	0.17	0.866 ± 0.003	× 1.1	0.83	0.098 ± 0.002	× 1.8
JT100	0.19	0.863 ± 0.003	× 1.1	0.83	0.116 ± 0.002	× 1.7
	L cut	new wh130 efficiency	improvement	L cut	new jt efficiency	reduction
JT20	0.04	0.876 ± 0.003	× 1.2	0.87	0.058 ± 0.001	× 3.2
JT50	0.16	0.860 ± 0.003	× 1.2	0.87	0.075 ± 0.002	× 2.2
JT70	0.17	0.859 ± 0.003	× 1.1	0.87	0.091 ± 0.002	× 2.0
JT100	0.19	0.857 ± 0.003	× 1.1	0.87	0.109 ± 0.002	× 1.8
	L cut	new wh140 efficiency	improvement	L cut	new jt efficiency	reduction
JT20	0.04	0.874 ± 0.002	× 1.2	0.88	0.057 ± 0.001	× 3.2
JT50	0.16	0.859 ± 0.003	× 1.2	0.88	0.073 ± 0.002	× 2.2
JT70	0.17	0.858 ± 0.003	× 1.2	0.88	0.089 ± 0.002	× 2.0
JT100	0.19	0.856 ± 0.003	× 1.1	0.88	0.106 ± 0.002	× 1.8
	L cut	new wh150 efficiency	improvement	L cut	new jt efficiency	reduction
JT20	0.04	0.869 ± 0.002	× 1.2	0.90	0.053 ± 0.001	× 3.5
JT50	0.16	0.855 ± 0.003	× 1.2	0.90	0.069 ± 0.002	× 2.4
JT70	0.17	0.855 ± 0.003	× 1.2	0.90	0.085 ± 0.002	× 2.1
JT100	0.19	0.853 ± 0.003	× 1.2	0.90	0.102 ± 0.002	× 1.9
	L cut	new wh170 efficiency	improvement	L cut	new jt efficiency	reduction
JT20	0.04	0.861 ± 0.003	× 1.2	0.93	0.045 ± 0.001	× 4.1
JT50	0.16	0.848 ± 0.003	× 1.2	0.93	0.062 ± 0.002	× 2.6
JT70	0.17	0.846 ± 0.003	× 1.2	0.93	0.076 ± 0.002	× 2.4
JT100	0.19	0.845 ± 0.003	× 1.2	0.93	0.093 ± 0.002	× 2.1
	L cut	new wh180 efficiency	improvement	L cut	new jt efficiency	reduction
JT20	0.04	0.864 ± 0.002	× 1.2	0.93	0.045 ± 0.001	× 4.1
JT50	0.16	0.851 ± 0.003	× 1.2	0.93	0.062 ± 0.002	× 2.6
JT70	0.17	0.850 ± 0.003	× 1.2	0.93	0.076 ± 0.002	× 2.4
JT100	0.19	0.849 ± 0.003	× 1.2	0.93	0.093 ± 0.002	× 2.1
	L cut	new wh190 efficiency	improvement	L cut	new jt efficiency	reduction
JT20	0.04	0.862 ± 0.002	× 1.2	0.92	0.048 ± 0.001	× 3.9
JT50	0.16	0.850 ± 0.002	× 1.2	0.92	0.064 ± 0.002	× 2.5
JT70	0.17	0.849 ± 0.002	× 1.2	0.92	0.080 ± 0.002	× 2.3
JT100	0.19	0.848 ± 0.003	× 1.2	0.92	0.097 ± 0.002	× 2.0
	L cut	new wh200 efficiency	improvement	L cut	new jt efficiency	reduction
JT20	0.04	0.859 ± 0.002	× 1.2	0.92	0.048 ± 0.001	× 3.9
JT50	0.16	0.846 ± 0.002	× 1.2	0.92	0.064 ± 0.002	× 2.5
JT70	0.17	0.845 ± 0.002	× 1.2	0.92	0.080 ± 0.002	× 2.3
JT100	0.19	0.843 ± 0.003	× 1.2	0.92	0.097 ± 0.002	× 2.0

Table 5: Efficiencies of the likelihood-based method for electron selection compared to the cut-based method at the same background efficiencies or the same signal efficiencies. The samples are higgs MC events and the signal PDFs are created from the higgs MC events.

Sample	Same background efficiency			Same signal efficiency		
	L cut	new wh110 efficiency	improvement	L cut	new jt efficiency	reduction
JT20	0.31	0.907 ± 0.002	$\times$ 1.2	0.95	0.065 ± 0.001	$\times$ 2.9
JT50	0.56	0.893 ± 0.003	$\times$ 1.1	0.95	0.075 ± 0.002	$\times$ 2.2
JT70	0.60	0.890 ± 0.003	$\times$ 1.1	0.95	0.091 ± 0.002	$\times$ 2.0
JT100	0.63	0.886 ± 0.003	$\times$ 1.1	0.95	0.112 ± 0.002	$\times$ 1.8
	L cut	new wh120 efficiency	improvement	L cut	new jt efficiency	reduction
JT20	0.31	0.901 ± 0.002	$\times$ 1.2	0.96	0.056 ± 0.001	$\times$ 3.3
JT50	0.58	0.883 ± 0.003	$\times$ 1.2	0.96	0.068 ± 0.002	$\times$ 2.4
JT70	0.62	0.880 ± 0.003	$\times$ 1.2	0.96	0.085 ± 0.002	$\times$ 2.1
JT100	0.66	0.876 ± 0.003	$\times$ 1.2	0.96	0.104 ± 0.002	$\times$ 1.9
	L cut	new wh130 efficiency	improvement	L cut	new jt efficiency	reduction
JT20	0.30	0.896 ± 0.002	$\times$ 1.2	0.96	0.054 ± 0.001	$\times$ 3.4
JT50	0.59	0.874 ± 0.003	$\times$ 1.2	0.96	0.066 ± 0.002	$\times$ 2.5
JT70	0.62	0.872 ± 0.003	$\times$ 1.2	0.96	0.083 ± 0.002	$\times$ 2.2
JT100	0.66	0.868 ± 0.003	$\times$ 1.2	0.96	0.102 ± 0.002	$\times$ 1.9
	L cut	new wh140 efficiency	improvement	L cut	new jt efficiency	reduction
JT20	0.29	0.895 ± 0.002	$\times$ 1.2	0.96	0.052 ± 0.001	$\times$ 3.6
JT50	0.58	0.875 ± 0.002	$\times$ 1.2	0.96	0.065 ± 0.002	$\times$ 2.5
JT70	0.62	0.871 ± 0.003	$\times$ 1.2	0.96	0.083 ± 0.002	$\times$ 2.2
JT100	0.66	0.867 ± 0.003	$\times$ 1.2	0.96	0.101 ± 0.002	$\times$ 1.9
	L cut	new wh150 efficiency	improvement	L cut	new jt efficiency	reduction
JT20	0.29	0.890 ± 0.002	$\times$ 1.2	0.96	0.050 ± 0.001	$\times$ 3.7
JT50	0.58	0.870 ± 0.002	$\times$ 1.2	0.96	0.064 ± 0.002	$\times$ 2.6
JT70	0.62	0.867 ± 0.003	$\times$ 1.2	0.96	0.081 ± 0.002	$\times$ 2.2
JT100	0.66	0.863 ± 0.003	$\times$ 1.2	0.96	0.099 ± 0.002	$\times$ 2.0

Table 6: Efficiencies of the likelihood-based method for electron selection compared to the cut-based method at the same background efficiencies or the same signal efficiencies. The samples are higgs MC events and the signal PDFs are created from the higgs MC events.

Sample	Same background efficiency			Same signal efficiency		
	L cut	new wh160 efficiency	improvement	L cut	new jt efficiency	reduction
JT20	0.27	0.892 ± 0.002	× 1.2	0.97	0.041 ± 0.001	× 4.5
JT50	0.59	0.869 ± 0.002	× 1.2	0.97	0.057 ± 0.002	× 2.9
JT70	0.63	0.866 ± 0.003	× 1.2	0.97	0.071 ± 0.002	× 2.5
JT100	0.67	0.862 ± 0.003	× 1.2	0.97	0.089 ± 0.002	× 2.2
	L cut	new wh170 efficiency	improvement	L cut	new jt efficiency	reduction
JT20	0.27	0.887 ± 0.002	× 1.2	0.96	0.046 ± 0.001	× 4.0
JT50	0.59	0.861 ± 0.003	× 1.2	0.96	0.064 ± 0.002	× 2.6
JT70	0.63	0.858 ± 0.003	× 1.2	0.96	0.080 ± 0.002	× 2.2
JT100	0.68	0.854 ± 0.003	× 1.2	0.96	0.098 ± 0.002	× 2.0
	L cut	new wh180 efficiency	improvement	L cut	new jt efficiency	reduction
JT20	0.26	0.891 ± 0.002	× 1.2	0.96	0.045 ± 0.001	× 4.1
JT50	0.58	0.867 ± 0.002	× 1.2	0.96	0.063 ± 0.002	× 2.6
JT70	0.63	0.863 ± 0.002	× 1.2	0.96	0.080 ± 0.002	× 2.3
JT100	0.67	0.859 ± 0.002	× 1.2	0.96	0.099 ± 0.002	× 2.0
	L cut	new wh190 efficiency	improvement	L cut	new jt efficiency	reduction
JT20	0.26	0.891 ± 0.002	× 1.2	0.96	0.045 ± 0.001	× 4.1
JT50	0.59	0.868 ± 0.002	× 1.2	0.96	0.063 ± 0.002	× 2.6
JT70	0.63	0.864 ± 0.002	× 1.2	0.96	0.081 ± 0.002	× 2.2
JT100	0.68	0.859 ± 0.002	× 1.2	0.96	0.100 ± 0.002	× 2.0
	L cut	new wh200 efficiency	improvement	L cut	new jt efficiency	reduction
JT20	0.26	0.889 ± 0.002	× 1.2	0.96	0.045 ± 0.001	× 4.1
JT50	0.59	0.865 ± 0.002	× 1.2	0.96	0.063 ± 0.002	× 2.6
JT70	0.64	0.861 ± 0.002	× 1.2	0.96	0.081 ± 0.002	× 2.2
JT100	0.69	0.855 ± 0.002	× 1.2	0.96	0.100 ± 0.002	× 2.0

Table 7: Efficiencies of the cut-based method for CMUP muon selection.

Sample	total	pass	efficiency
MU	29068	23063	0.793 ± 0.002
Wh110	9639	7282	0.755 ± 0.004
Wh120	10089	7724	0.766 ± 0.004
Wh130	10710	8340	0.779 ± 0.004
Wh140	11216	8848	0.789 ± 0.004
Wh150	11413	8963	0.785 ± 0.004
Wh160	11522	9103	0.790 ± 0.004
Wh170	11864	9384	0.791 ± 0.004
Wh180	12447	9838	0.790 ± 0.004
Wh190	13239	10550	0.797 ± 0.003
Wh200	13698	10836	0.791 ± 0.003
JT20	8773	2324	0.265 ± 0.005
JT50	4043	916	0.227 ± 0.007
JT70	5823	1367	0.235 ± 0.006
JT100	6137	1460	0.238 ± 0.005

Table 8: Efficiencies of the likelihood-based method for CMUP muon selection compared to the cut-based method at the same background efficiencies or the same signal efficiencies. The signal PDFs are created from Z events.

Sample	Same background efficiency			Same signal efficiency		
	L cut	new mu efficiency	improvement	L cut	new jt efficiency	reduction
JT20	0.34	0.934 ± 0.001	× 1.2	0.73	0.141 ± 0.004	× 1.9
JT50	0.49	0.894 ± 0.002	× 1.1	0.73	0.147 ± 0.006	× 1.5
JT70	0.48	0.897 ± 0.002	× 1.1	0.73	0.154 ± 0.005	× 1.5
JT100	0.58	0.863 ± 0.002	× 1.1	0.73	0.183 ± 0.005	× 1.3
	L cut	new wh110 efficiency	improvement	L cut	new jt efficiency	reduction
JT20	0.34	0.759 ± 0.004	× 1.0	0.35	0.261 ± 0.005	× 1.0
JT50	0.49	0.716 ± 0.005	× 0.9	0.35	0.275 ± 0.007	× 0.8
JT70	0.48	0.719 ± 0.005	× 1.0	0.35	0.284 ± 0.006	× 0.8
JT100	0.58	0.687 ± 0.005	× 0.9	0.35	0.321 ± 0.006	× 0.7
	L cut	new wh160 efficiency	improvement	L cut	new jt efficiency	reduction
JT20	0.34	0.867 ± 0.003	× 1.1	0.66	0.163 ± 0.004	× 1.6
JT50	0.49	0.835 ± 0.003	× 1.1	0.66	0.174 ± 0.006	× 1.3
JT70	0.48	0.838 ± 0.003	× 1.1	0.66	0.176 ± 0.005	× 1.3
JT100	0.58	0.814 ± 0.004	× 1.0	0.66	0.206 ± 0.005	× 1.2

Table 9: Efficiencies of the likelihood-based method for CMUP muon selection compared to the cut-based method at the same background efficiencies or the same signal efficiencies. The samples are higgs MC events of masses other than 110 GeV/c^2 and 160 GeV/c^2. The signal PDFs are created from Z events.

Sample	Same background efficiency			Same signal efficiency		
	L cut	new wh120 efficiency	improvement	L cut	new jt efficiency	reduction
JT20	0.34	0.793 ± 0.004	$\times$ 1.0	0.43	0.235 ± 0.005	$\times$ 1.1
JT50	0.49	0.750 ± 0.004	$\times$ 1.0	0.43	0.248 ± 0.007	$\times$ 0.9
JT70	0.48	0.753 ± 0.004	$\times$ 1.0	0.43	0.251 ± 0.006	$\times$ 0.9
JT100	0.58	0.722 ± 0.004	$\times$ 0.9	0.43	0.289 ± 0.006	$\times$ 0.8
	L cut	new wh130 efficiency	improvement	L cut	new jt efficiency	reduction
JT20	0.34	0.817 ± 0.004	$\times$ 1.0	0.49	0.216 ± 0.004	$\times$ 1.2
JT50	0.49	0.780 ± 0.004	$\times$ 1.0	0.49	0.226 ± 0.007	$\times$ 1.0
JT70	0.48	0.784 ± 0.004	$\times$ 1.0	0.49	0.230 ± 0.006	$\times$ 1.0
JT100	0.58	0.755 ± 0.004	$\times$ 1.0	0.49	0.266 ± 0.006	$\times$ 0.9
	L cut	new wh140 efficiency	improvement	L cut	new jt efficiency	reduction
JT20	0.34	0.835 ± 0.004	$\times$ 1.1	0.52	0.205 ± 0.004	$\times$ 1.3
JT50	0.49	0.798 ± 0.004	$\times$ 1.0	0.52	0.214 ± 0.006	$\times$ 1.1
JT70	0.48	0.800 ± 0.004	$\times$ 1.0	0.52	0.222 ± 0.005	$\times$ 1.1
JT100	0.58	0.774 ± 0.004	$\times$ 1.0	0.52	0.256 ± 0.006	$\times$ 0.9
	L cut	new wh150 efficiency	improvement	L cut	new jt efficiency	reduction
JT20	0.34	0.855 ± 0.003	$\times$ 1.1	0.61	0.179 ± 0.004	$\times$ 1.5
JT50	0.49	0.817 ± 0.004	$\times$ 1.0	0.61	0.188 ± 0.006	$\times$ 1.2
JT70	0.48	0.819 ± 0.004	$\times$ 1.0	0.61	0.191 ± 0.005	$\times$ 1.2
JT100	0.58	0.794 ± 0.004	$\times$ 1.0	0.61	0.225 ± 0.005	$\times$ 1.1
	L cut	new wh170 efficiency	improvement	L cut	new jt efficiency	reduction
JT20	0.34	0.876 ± 0.003	$\times$ 1.1	0.67	0.159 ± 0.004	$\times$ 1.7
JT50	0.49	0.845 ± 0.003	$\times$ 1.1	0.67	0.171 ± 0.006	$\times$ 1.3
JT70	0.48	0.847 ± 0.003	$\times$ 1.1	0.67	0.173 ± 0.005	$\times$ 1.4
JT100	0.58	0.821 ± 0.004	$\times$ 1.0	0.67	0.203 ± 0.005	$\times$ 1.2
	L cut	new wh180 efficiency	improvement	L cut	new jt efficiency	reduction
JT20	0.34	0.885 ± 0.003	$\times$ 1.1	0.70	0.150 ± 0.004	$\times$ 1.8
JT50	0.49	0.853 ± 0.003	$\times$ 1.1	0.70	0.158 ± 0.006	$\times$ 1.4
JT70	0.48	0.855 ± 0.003	$\times$ 1.1	0.70	0.163 ± 0.005	$\times$ 1.4
JT100	0.58	0.831 ± 0.003	$\times$ 1.1	0.70	0.193 ± 0.005	$\times$ 1.2
	L cut	new wh190 efficiency	improvement	L cut	new jt efficiency	reduction
JT20	0.34	0.889 ± 0.003	$\times$ 1.1	0.71	0.147 ± 0.004	$\times$ 1.8
JT50	0.49	0.858 ± 0.003	$\times$ 1.1	0.71	0.156 ± 0.006	$\times$ 1.5
JT70	0.48	0.860 ± 0.003	$\times$ 1.1	0.71	0.160 ± 0.005	$\times$ 1.5
JT100	0.58	0.837 ± 0.003	$\times$ 1.1	0.71	0.191 ± 0.005	$\times$ 1.2
	L cut	new wh200 efficiency	improvement	L cut	new jt efficiency	reduction
JT20	0.34	0.890 ± 0.003	$\times$ 1.1	0.73	0.141 ± 0.004	$\times$ 1.9
JT50	0.49	0.862 ± 0.003	$\times$ 1.1	0.73	0.147 ± 0.006	$\times$ 1.5
JT70	0.48	0.865 ± 0.003	$\times$ 1.1	0.73	0.154 ± 0.005	$\times$ 1.5
JT100	0.58	0.841 ± 0.003	$\times$ 1.1	0.73	0.183 ± 0.005	$\times$ 1.3

Table 10: Efficiencies of the likelihood-based method for CMUP muon selection compared to the cut-based method at the same background efficiencies or the same signal efficiencies. The samples are higgs MC events and the signal PDFs are created from the higgs MC events.

Sample	Same background efficiency			Same signal efficiency		
	L cut	new wh110 efficiency	improvement	L cut	new jt efficiency	reduction
`JT20`	0.60	0.783 ± 0.004	$\times$ 1.0	0.64	0.240 ± 0.005	$\times$ 1.1
`JT50`	0.64	0.759 ± 0.004	$\times$ 1.0	0.64	0.226 ± 0.007	$\times$ 1.0
`JT70`	0.65	0.755 ± 0.004	$\times$ 1.0	0.64	0.238 ± 0.006	$\times$ 1.0
`JT100`	0.68	0.735 ± 0.004	$\times$ 1.0	0.64	0.260 ± 0.006	$\times$ 0.9
	L cut	new wh120 efficiency	improvement	L cut	new jt efficiency	reduction
`JT20`	0.57	0.814 ± 0.004	$\times$ 1.1	0.66	0.218 ± 0.004	$\times$ 1.2
`JT50`	0.64	0.783 ± 0.004	$\times$ 1.0	0.66	0.213 ± 0.006	$\times$ 1.1
`JT70`	0.63	0.788 ± 0.004	$\times$ 1.0	0.66	0.221 ± 0.005	$\times$ 1.1
`JT100`	0.67	0.765 ± 0.004	$\times$ 1.0	0.66	0.241 ± 0.005	$\times$ 1.0
	L cut	new wh130 efficiency	improvement	L cut	new jt efficiency	reduction
`JT20`	0.53	0.841 ± 0.004	$\times$ 1.1	0.66	0.208 ± 0.004	$\times$ 1.3
`JT50`	0.62	0.803 ± 0.004	$\times$ 1.0	0.66	0.210 ± 0.006	$\times$ 1.1
`JT70`	0.62	0.803 ± 0.004	$\times$ 1.0	0.66	0.216 ± 0.005	$\times$ 1.1
`JT100`	0.67	0.778 ± 0.004	$\times$ 1.0	0.66	0.238 ± 0.005	$\times$ 1.0
	L cut	new wh140 efficiency	improvement	L cut	new jt efficiency	reduction
`JT20`	0.51	0.852 ± 0.003	$\times$ 1.1	0.67	0.194 ± 0.004	$\times$ 1.4
`JT50`	0.61	0.816 ± 0.004	$\times$ 1.0	0.67	0.200 ± 0.006	$\times$ 1.1
`JT70`	0.62	0.812 ± 0.004	$\times$ 1.0	0.67	0.209 ± 0.005	$\times$ 1.1
`JT100`	0.66	0.794 ± 0.004	$\times$ 1.0	0.67	0.232 ± 0.005	$\times$ 1.0
	L cut	new wh150 efficiency	improvement	L cut	new jt efficiency	reduction
`JT20`	0.48	0.870 ± 0.003	$\times$ 1.1	0.70	0.179 ± 0.004	$\times$ 1.5
`JT50`	0.60	0.831 ± 0.004	$\times$ 1.1	0.70	0.183 ± 0.006	$\times$ 1.2
`JT70`	0.61	0.829 ± 0.004	$\times$ 1.1	0.70	0.197 ± 0.005	$\times$ 1.2
`JT100`	0.66	0.810 ± 0.004	$\times$ 1.0	0.70	0.219 ± 0.005	$\times$ 1.1

Table 11: Efficiencies of the likelihood-based method for CMUP muon selection compared to the cut-based method at the same background efficiencies or the same signal efficiencies. The samples are higgs MC events and the signal PDFs are created from the higgs MC events.

Sample	Same background efficiency			Same signal efficiency		
	L cut	new wh160 efficiency	improvement	L cut	new jt efficiency	reduction
JT20	0.44	0.879 ± 0.003	$\times$ 1.1	0.71	0.168 ± 0.004	$\times$ 1.6
JT50	0.59	0.837 ± 0.003	$\times$ 1.1	0.71	0.174 ± 0.006	$\times$ 1.3
JT70	0.58	0.840 ± 0.003	$\times$ 1.1	0.71	0.187 ± 0.005	$\times$ 1.3
JT100	0.64	0.822 ± 0.004	$\times$ 1.0	0.71	0.208 ± 0.005	$\times$ 1.1
	L cut	new wh170 efficiency	improvement	L cut	new jt efficiency	reduction
JT20	0.43	0.887 ± 0.003	$\times$ 1.1	0.72	0.162 ± 0.004	$\times$ 1.6
JT50	0.59	0.844 ± 0.003	$\times$ 1.1	0.72	0.170 ± 0.006	$\times$ 1.3
JT70	0.58	0.847 ± 0.003	$\times$ 1.1	0.72	0.182 ± 0.005	$\times$ 1.3
JT100	0.65	0.823 ± 0.004	$\times$ 1.0	0.72	0.205 ± 0.005	$\times$ 1.2
	L cut	new wh180 efficiency	improvement	L cut	new jt efficiency	reduction
JT20	0.41	0.893 ± 0.003	$\times$ 1.1	0.74	0.148 ± 0.004	$\times$ 1.8
JT50	0.56	0.856 ± 0.003	$\times$ 1.1	0.74	0.159 ± 0.006	$\times$ 1.4
JT70	0.57	0.854 ± 0.003	$\times$ 1.1	0.74	0.171 ± 0.005	$\times$ 1.4
JT100	0.64	0.833 ± 0.003	$\times$ 1.1	0.74	0.194 ± 0.005	$\times$ 1.2
	L cut	new wh190 efficiency	improvement	L cut	new jt efficiency	reduction
JT20	0.40	0.895 ± 0.003	$\times$ 1.1	0.73	0.149 ± 0.004	$\times$ 1.8
JT50	0.56	0.857 ± 0.003	$\times$ 1.1	0.73	0.159 ± 0.006	$\times$ 1.4
JT70	0.57	0.853 ± 0.003	$\times$ 1.1	0.73	0.172 ± 0.005	$\times$ 1.4
JT100	0.63	0.836 ± 0.003	$\times$ 1.0	0.73	0.195 ± 0.005	$\times$ 1.2
	L cut	new wh200 efficiency	improvement	L cut	new jt efficiency	reduction
JT20	0.39	0.898 ± 0.003	$\times$ 1.1	0.74	0.144 ± 0.004	$\times$ 1.8
JT50	0.55	0.859 ± 0.003	$\times$ 1.1	0.74	0.155 ± 0.006	$\times$ 1.5
JT70	0.56	0.857 ± 0.003	$\times$ 1.1	0.74	0.169 ± 0.005	$\times$ 1.4
JT100	0.62	0.838 ± 0.003	$\times$ 1.1	0.74	0.192 ± 0.005	$\times$ 1.2

Table 12: Efficiencies of the cut-based method for CMX muon selection.

Sample	total	pass	efficiency
MU	18836	16356	0.868 ± 0.002
Wh110	4853	3902	0.804 ± 0.006
Wh120	5250	4243	0.808 ± 0.005
Wh130	5559	4583	0.824 ± 0.005
Wh140	5773	4776	0.827 ± 0.005
Wh150	6014	4872	0.810 ± 0.005
Wh160	6079	5074	0.835 ± 0.005
Wh170	6124	5086	0.831 ± 0.005
Wh180	6442	5370	0.834 ± 0.005
Wh190	6827	5606	0.821 ± 0.005
Wh200	6881	5687	0.826 ± 0.005
JT20	6955	2007	0.289 ± 0.005
JT50	2944	817	0.278 ± 0.008
JT70	4107	1159	0.282 ± 0.007
JT100	4069	1228	0.302 ± 0.007

Table 13: Efficiencies of the likelihood-based method for CMX muon selection compared to the cut-based method at the same background efficiencies or the same signal efficiencies. The signal PDFs are created from Z events.

Sample	Same background efficiency			Same signal efficiency		
	L cut	new mu efficiency	improvement	L cut	new jt efficiency	reduction
JT20	0.19	0.967 ± 0.001	$\times$ 1.1	0.58	0.174 ± 0.005	$\times$ 1.7
JT50	0.27	0.956 ± 0.001	$\times$ 1.1	0.58	0.180 ± 0.007	$\times$ 1.5
JT70	0.28	0.954 ± 0.002	$\times$ 1.1	0.58	0.183 ± 0.006	$\times$ 1.5
JT100	0.25	0.959 ± 0.001	$\times$ 1.1	0.58	0.196 ± 0.006	$\times$ 1.5
	L cut	new wh110 efficiency	improvement	L cut	new jt efficiency	reduction
JT20	0.19	0.851 ± 0.005	$\times$ 1.1	0.35	0.238 ± 0.005	$\times$ 1.2
JT50	0.27	0.827 ± 0.005	$\times$ 1.0	0.35	0.252 ± 0.008	$\times$ 1.1
JT70	0.28	0.825 ± 0.005	$\times$ 1.0	0.35	0.260 ± 0.007	$\times$ 1.1
JT100	0.25	0.833 ± 0.005	$\times$ 1.0	0.35	0.270 ± 0.007	$\times$ 1.1
	L cut	new wh160 efficiency	improvement	L cut	new jt efficiency	reduction
JT20	0.19	0.922 ± 0.003	$\times$ 1.1	0.48	0.198 ± 0.005	$\times$ 1.5
JT50	0.27	0.904 ± 0.004	$\times$ 1.1	0.48	0.203 ± 0.007	$\times$ 1.4
JT70	0.28	0.901 ± 0.004	$\times$ 1.1	0.48	0.216 ± 0.006	$\times$ 1.3
JT100	0.25	0.910 ± 0.004	$\times$ 1.1	0.48	0.225 ± 0.007	$\times$ 1.3

Table 14: Efficiencies of the likelihood-based method for CMX muon selection compared to the cut-based method at the same background efficiencies or the same signal efficiencies. The samples are higgs MC events of masses other than 110 GeV/c^2 and 160 GeV/c^2. The signal PDFs are created from Z events.

Sample	Same background efficiency			Same signal efficiency		
	L cut	new wh120 efficiency	improvement	L cut	new jt efficiency	reduction
JT20	0.19	0.861 ± 0.005	× 1.1	0.37	0.229 ± 0.005	× 1.3
JT50	0.27	0.839 ± 0.005	× 1.0	0.37	0.245 ± 0.008	× 1.1
JT70	0.28	0.837 ± 0.005	× 1.0	0.37	0.253 ± 0.007	× 1.1
JT100	0.25	0.845 ± 0.005	× 1.0	0.37	0.264 ± 0.007	× 1.1
	L cut	new wh130 efficiency	improvement	L cut	new jt efficiency	reduction
JT20	0.19	0.886 ± 0.004	× 1.1	0.40	0.221 ± 0.005	× 1.3
JT50	0.27	0.864 ± 0.005	× 1.0	0.40	0.230 ± 0.008	× 1.2
JT70	0.28	0.861 ± 0.005	× 1.0	0.40	0.244 ± 0.007	× 1.2
JT100	0.25	0.870 ± 0.005	× 1.1	0.40	0.253 ± 0.007	× 1.2
	L cut	new wh140 efficiency	improvement	L cut	new jt efficiency	reduction
JT20	0.19	0.898 ± 0.004	× 1.1	0.41	0.218 ± 0.005	× 1.3
JT50	0.27	0.873 ± 0.004	× 1.1	0.41	0.226 ± 0.008	× 1.2
JT70	0.28	0.870 ± 0.004	× 1.1	0.41	0.241 ± 0.007	× 1.2
JT100	0.25	0.878 ± 0.004	× 1.1	0.41	0.249 ± 0.007	× 1.2
	L cut	new wh150 efficiency	improvement	L cut	new jt efficiency	reduction
JT20	0.19	0.899 ± 0.004	× 1.1	0.47	0.200 ± 0.005	× 1.4
JT50	0.27	0.879 ± 0.004	× 1.1	0.47	0.206 ± 0.007	× 1.4
JT70	0.28	0.876 ± 0.004	× 1.1	0.47	0.218 ± 0.006	× 1.3
JT100	0.25	0.883 ± 0.004	× 1.1	0.47	0.230 ± 0.007	× 1.3
	L cut	new wh170 efficiency	improvement	L cut	new jt efficiency	reduction
JT20	0.19	0.920 ± 0.003	× 1.1	0.50	0.193 ± 0.005	× 1.5
JT50	0.27	0.902 ± 0.004	× 1.1	0.50	0.201 ± 0.007	× 1.4
JT70	0.28	0.901 ± 0.004	× 1.1	0.50	0.210 ± 0.006	× 1.3
JT100	0.25	0.906 ± 0.004	× 1.1	0.50	0.220 ± 0.006	× 1.4
	L cut	new wh180 efficiency	improvement	L cut	new jt efficiency	reduction
JT20	0.19	0.926 ± 0.003	× 1.1	0.51	0.192 ± 0.005	× 1.5
JT50	0.27	0.910 ± 0.004	× 1.1	0.51	0.199 ± 0.007	× 1.4
JT70	0.28	0.906 ± 0.004	× 1.1	0.51	0.206 ± 0.006	× 1.4
JT100	0.25	0.914 ± 0.003	× 1.1	0.51	0.218 ± 0.006	× 1.4
	L cut	new wh190 efficiency	improvement	L cut	new jt efficiency	reduction
JT20	0.19	0.925 ± 0.003	× 1.1	0.54	0.186 ± 0.005	× 1.6
JT50	0.27	0.908 ± 0.003	× 1.1	0.54	0.190 ± 0.007	× 1.5
JT70	0.28	0.906 ± 0.004	× 1.1	0.54	0.197 ± 0.006	× 1.4
JT100	0.25	0.911 ± 0.003	× 1.1	0.54	0.209 ± 0.006	× 1.4
	L cut	new wh200 efficiency	improvement	L cut	new jt efficiency	reduction
JT20	0.19	0.927 ± 0.003	× 1.1	0.54	0.186 ± 0.005	× 1.6
JT50	0.27	0.913 ± 0.003	× 1.1	0.54	0.190 ± 0.007	× 1.5
JT70	0.28	0.911 ± 0.003	× 1.1	0.54	0.197 ± 0.006	× 1.4
JT100	0.25	0.916 ± 0.003	× 1.1	0.54	0.209 ± 0.006	× 1.4

Table 15: Efficiencies of the likelihood-based method for CMX muon selection compared to the cut-based method at the same background efficiencies or the same signal efficiencies. The samples are higgs MC events and the signal PDFs are created from the higgs MC events.

Sample	Same background efficiency			Same signal efficiency		
	L cut	new wh110 efficiency	improvement	L cut	new jt efficiency	reduction
JT20	0.44	0.883 ± 0.005	× 1.1	0.56	0.216 ± 0.005	× 1.3
JT50	0.49	0.855 ± 0.005	× 1.1	0.56	0.233 ± 0.008	× 1.2
JT70	0.48	0.862 ± 0.005	× 1.1	0.56	0.243 ± 0.007	× 1.2
JT100	0.47	0.868 ± 0.005	× 1.1	0.56	0.254 ± 0.007	× 1.2
	L cut	new wh120 efficiency	improvement	L cut	new jt efficiency	reduction
JT20	0.43	0.899 ± 0.004	× 1.1	0.58	0.207 ± 0.005	× 1.4
JT50	0.48	0.872 ± 0.005	× 1.1	0.58	0.226 ± 0.008	× 1.2
JT70	0.48	0.872 ± 0.005	× 1.1	0.58	0.231 ± 0.007	× 1.2
JT100	0.48	0.872 ± 0.005	× 1.1	0.58	0.247 ± 0.007	× 1.2
	L cut	new wh130 efficiency	improvement	L cut	new jt efficiency	reduction
JT20	0.40	0.910 ± 0.004	× 1.1	0.56	0.208 ± 0.005	× 1.4
JT50	0.46	0.886 ± 0.004	× 1.1	0.56	0.222 ± 0.008	× 1.2
JT70	0.47	0.883 ± 0.004	× 1.1	0.56	0.230 ± 0.007	× 1.2
JT100	0.47	0.883 ± 0.004	× 1.1	0.56	0.247 ± 0.007	× 1.2
	L cut	new wh140 efficiency	improvement	L cut	new jt efficiency	reduction
JT20	0.40	0.922 ± 0.004	× 1.1	0.58	0.201 ± 0.005	× 1.4
JT50	0.46	0.897 ± 0.004	× 1.1	0.58	0.219 ± 0.008	× 1.3
JT70	0.47	0.893 ± 0.004	× 1.1	0.58	0.225 ± 0.007	× 1.3
JT100	0.46	0.897 ± 0.004	× 1.1	0.58	0.243 ± 0.007	× 1.2
	L cut	new wh150 efficiency	improvement	L cut	new jt efficiency	reduction
JT20	0.38	0.914 ± 0.004	× 1.1	0.59	0.183 ± 0.005	× 1.6
JT50	0.45	0.887 ± 0.004	× 1.1	0.59	0.202 ± 0.007	× 1.4
JT70	0.46	0.884 ± 0.004	× 1.1	0.59	0.210 ± 0.006	× 1.3
JT100	0.47	0.881 ± 0.004	× 1.1	0.59	0.227 ± 0.007	× 1.3

Table 16: Efficiencies of the likelihood-based method for CMX muon selection compared to the cut-based method at the same background efficiencies or the same signal efficiencies. The samples are higgs MC events and the signal PDFs are created from the higgs MC events.

Sample	Same background efficiency			Same signal efficiency		
	L cut	new wh160 efficiency	improvement	L cut	new jt efficiency	reduction
`JT20`	0.36	0.936 ± 0.003	$\times$ 1.1	0.58	0.186 ± 0.005	$\times$ 1.6
`JT50`	0.42	0.917 ± 0.004	$\times$ 1.1	0.58	0.206 ± 0.007	$\times$ 1.3
`JT70`	0.44	0.910 ± 0.004	$\times$ 1.1	0.58	0.210 ± 0.006	$\times$ 1.3
`JT100`	0.44	0.910 ± 0.004	$\times$ 1.1	0.58	0.225 ± 0.007	$\times$ 1.3
	L cut	new wh170 efficiency	improvement	L cut	new jt efficiency	reduction
`JT20`	0.36	0.934 ± 0.003	$\times$ 1.1	0.60	0.176 ± 0.005	$\times$ 1.6
`JT50`	0.42	0.914 ± 0.004	$\times$ 1.1	0.60	0.197 ± 0.007	$\times$ 1.4
`JT70`	0.43	0.911 ± 0.004	$\times$ 1.1	0.60	0.199 ± 0.006	$\times$ 1.4
`JT100`	0.44	0.909 ± 0.004	$\times$ 1.1	0.60	0.220 ± 0.006	$\times$ 1.4
	L cut	new wh180 efficiency	improvement	L cut	new jt efficiency	reduction
`JT20`	0.34	0.941 ± 0.003	$\times$ 1.1	0.58	0.177 ± 0.005	$\times$ 1.6
`JT50`	0.41	0.917 ± 0.003	$\times$ 1.1	0.58	0.195 ± 0.007	$\times$ 1.4
`JT70`	0.42	0.912 ± 0.004	$\times$ 1.1	0.58	0.204 ± 0.006	$\times$ 1.4
`JT100`	0.43	0.909 ± 0.004	$\times$ 1.1	0.58	0.222 ± 0.007	$\times$ 1.4
	L cut	new wh190 efficiency	improvement	L cut	new jt efficiency	reduction
`JT20`	0.32	0.942 ± 0.003	$\times$ 1.1	0.61	0.171 ± 0.005	$\times$ 1.7
`JT50`	0.41	0.916 ± 0.003	$\times$ 1.1	0.61	0.188 ± 0.007	$\times$ 1.5
`JT70`	0.43	0.910 ± 0.003	$\times$ 1.1	0.61	0.193 ± 0.006	$\times$ 1.5
`JT100`	0.43	0.910 ± 0.003	$\times$ 1.1	0.61	0.213 ± 0.006	$\times$ 1.4
	L cut	new wh200 efficiency	improvement	L cut	new jt efficiency	reduction
`JT20`	0.33	0.941 ± 0.003	$\times$ 1.1	0.60	0.165 ± 0.004	$\times$ 1.8
`JT50`	0.40	0.921 ± 0.003	$\times$ 1.1	0.60	0.186 ± 0.007	$\times$ 1.5
`JT70`	0.42	0.916 ± 0.003	$\times$ 1.1	0.60	0.189 ± 0.006	$\times$ 1.5
`JT100`	0.42	0.916 ± 0.003	$\times$ 1.1	0.60	0.211 ± 0.006	$\times$ 1.4

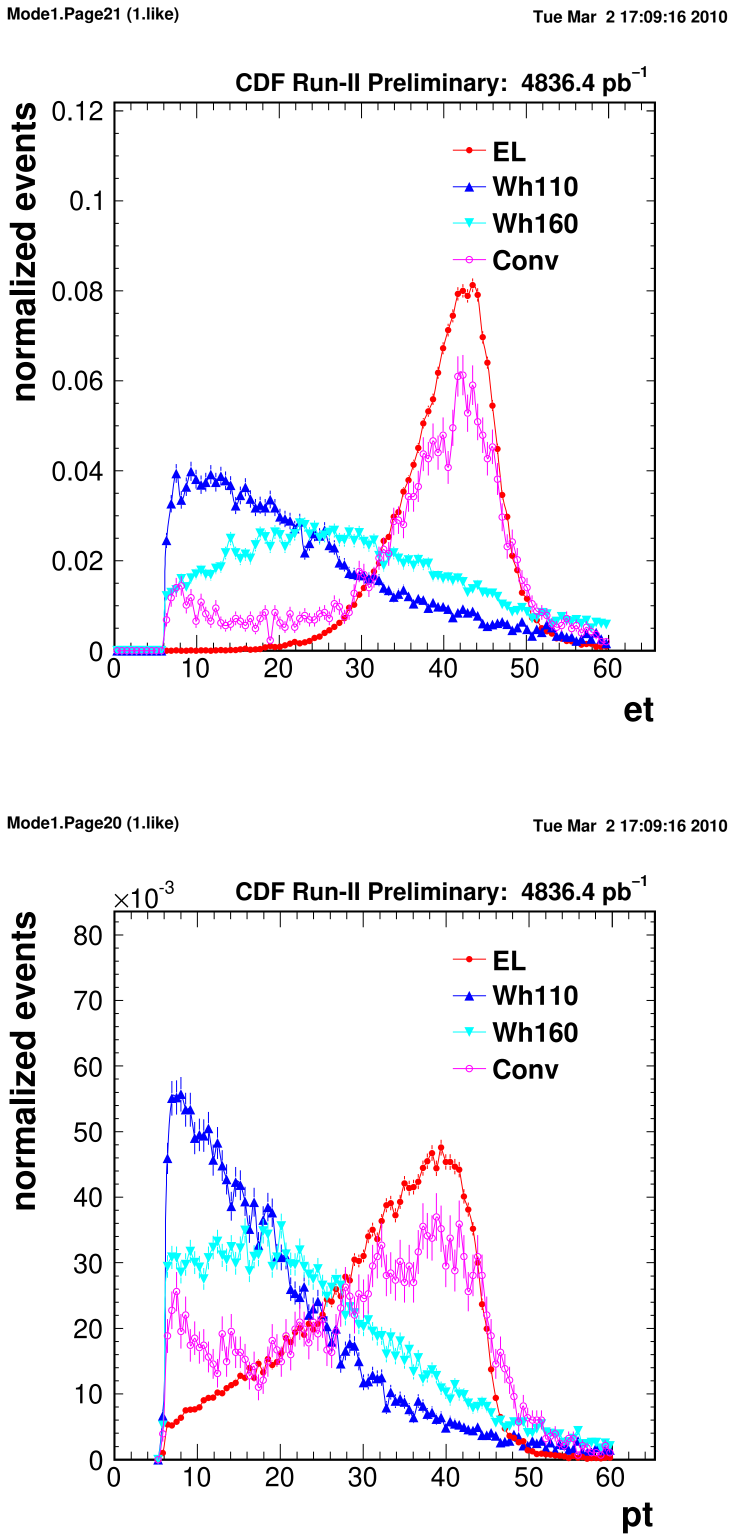

Figure 1: The E_T (top) and p_T (bottom) spectra of electrons for the samples of Z, photon conversions, and higgs Monte Carlos.

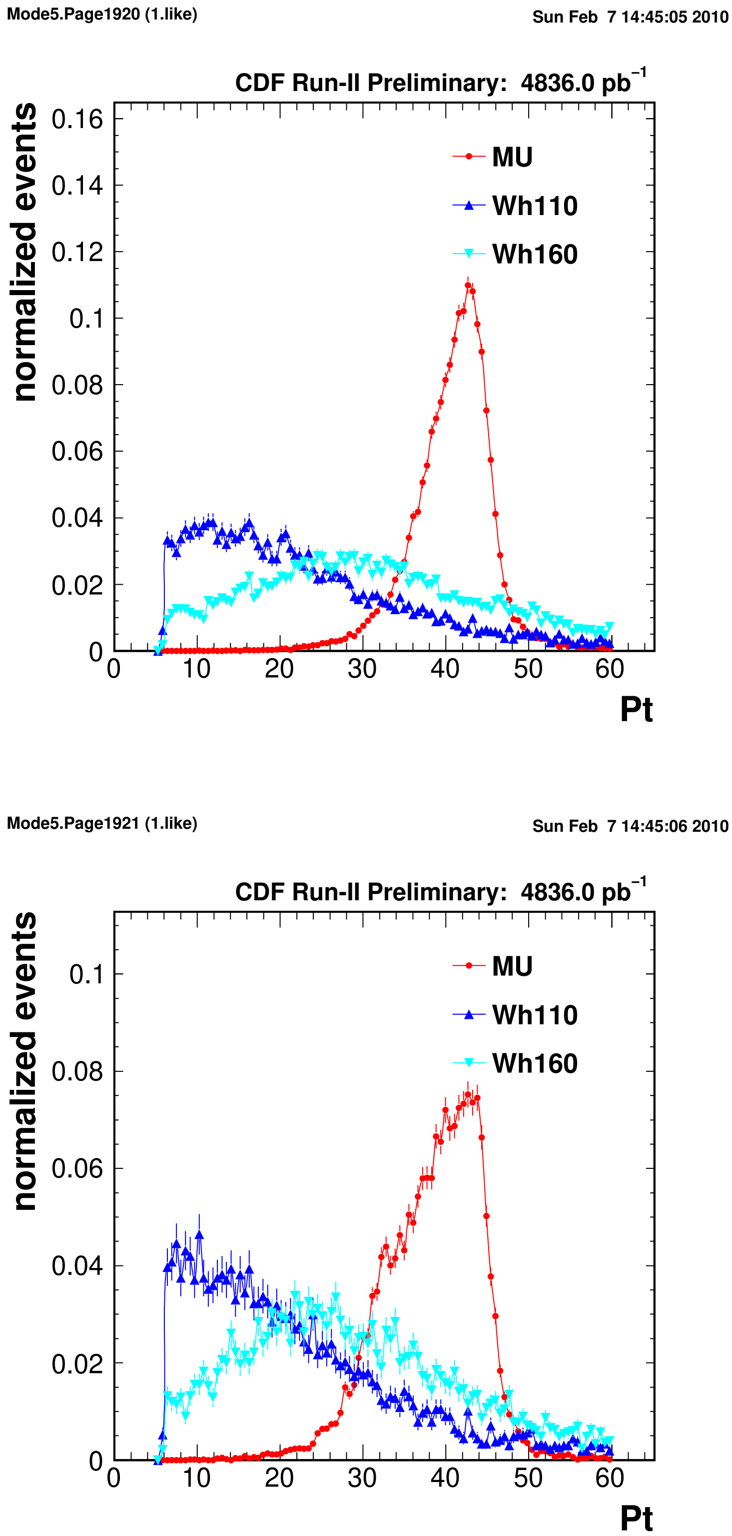

Figure 2: The p_T spectra of CMUP muons (top) and CMX muons (bottom) for the samples of Z and higgs Monte Carlos.

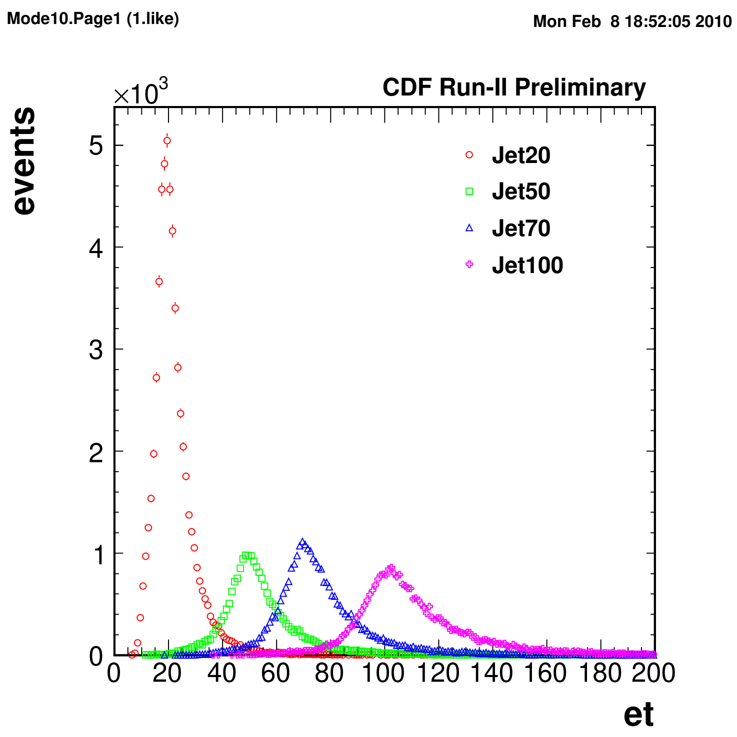

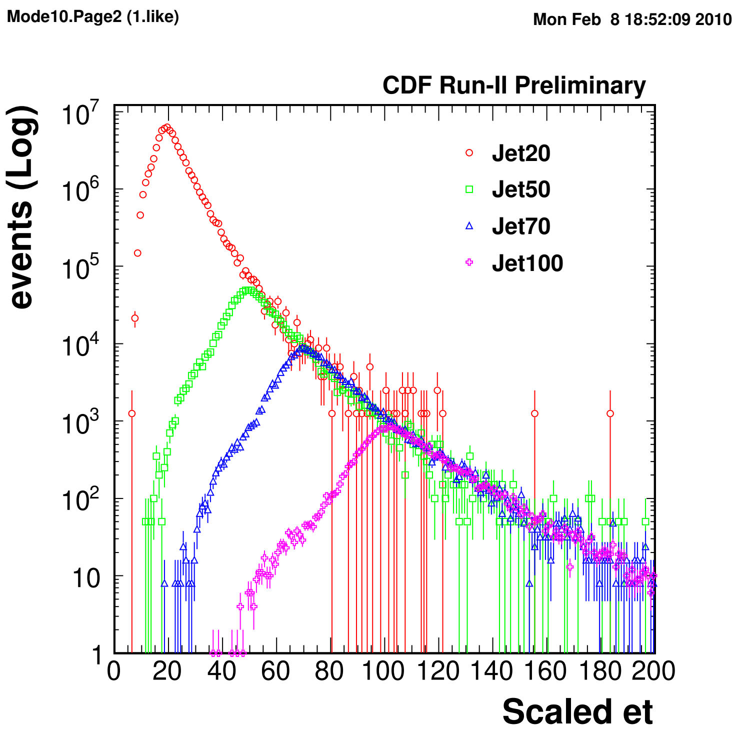

Figure 3: Inclusive jet E_T spectra for different jet triggers. The background PDFs are made with pre-scale weighted jet samples: $\times 1250$ for `Jet20`, $\times 50$ for `Jet50`, $\times 8$ for `Jet70`, and $\times 1$ for `Jet100`.

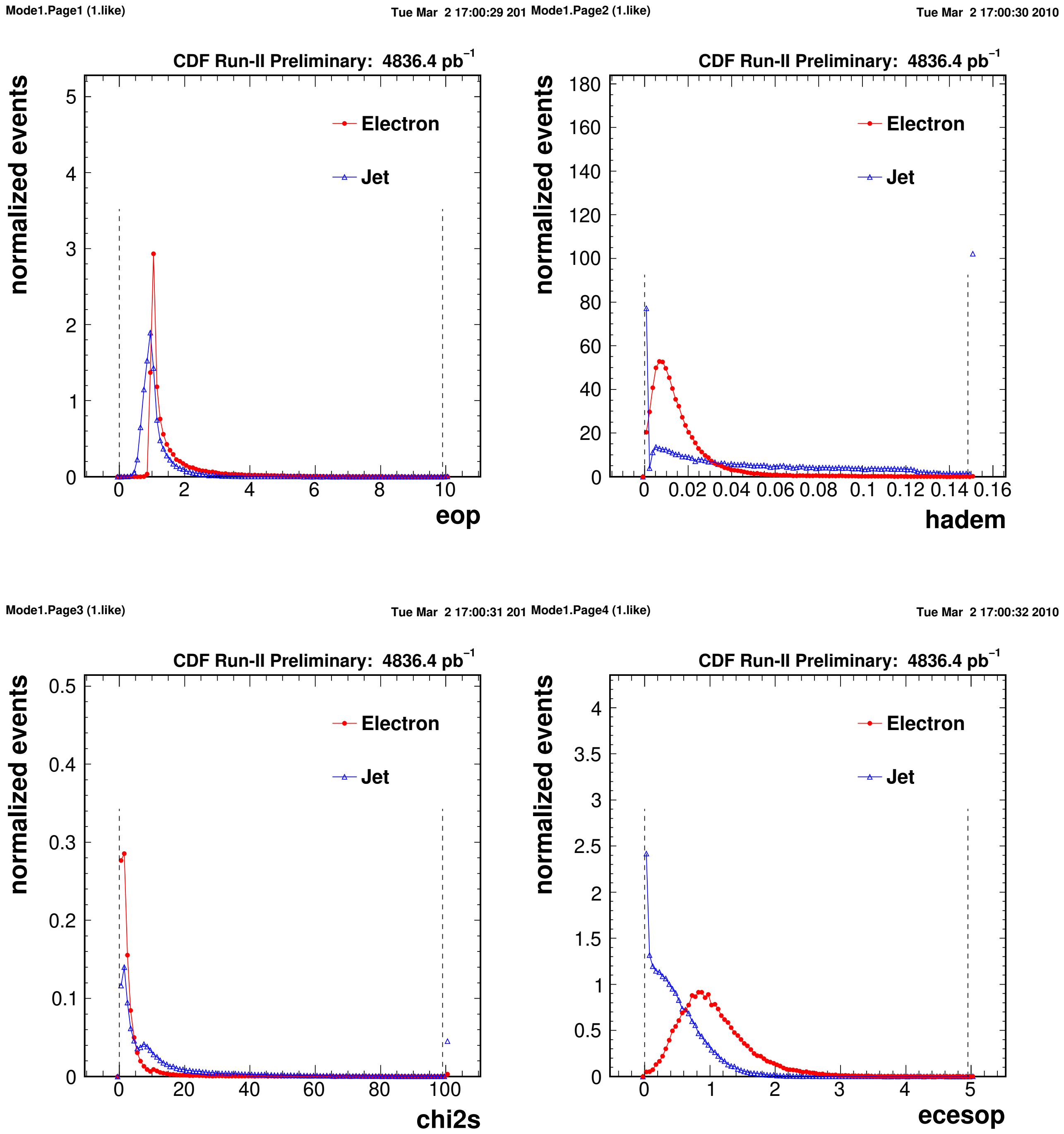

Figure 4: Normalized distributions of the identification variables for electrons from Z decays compared to those for electron candidates in jet samples.

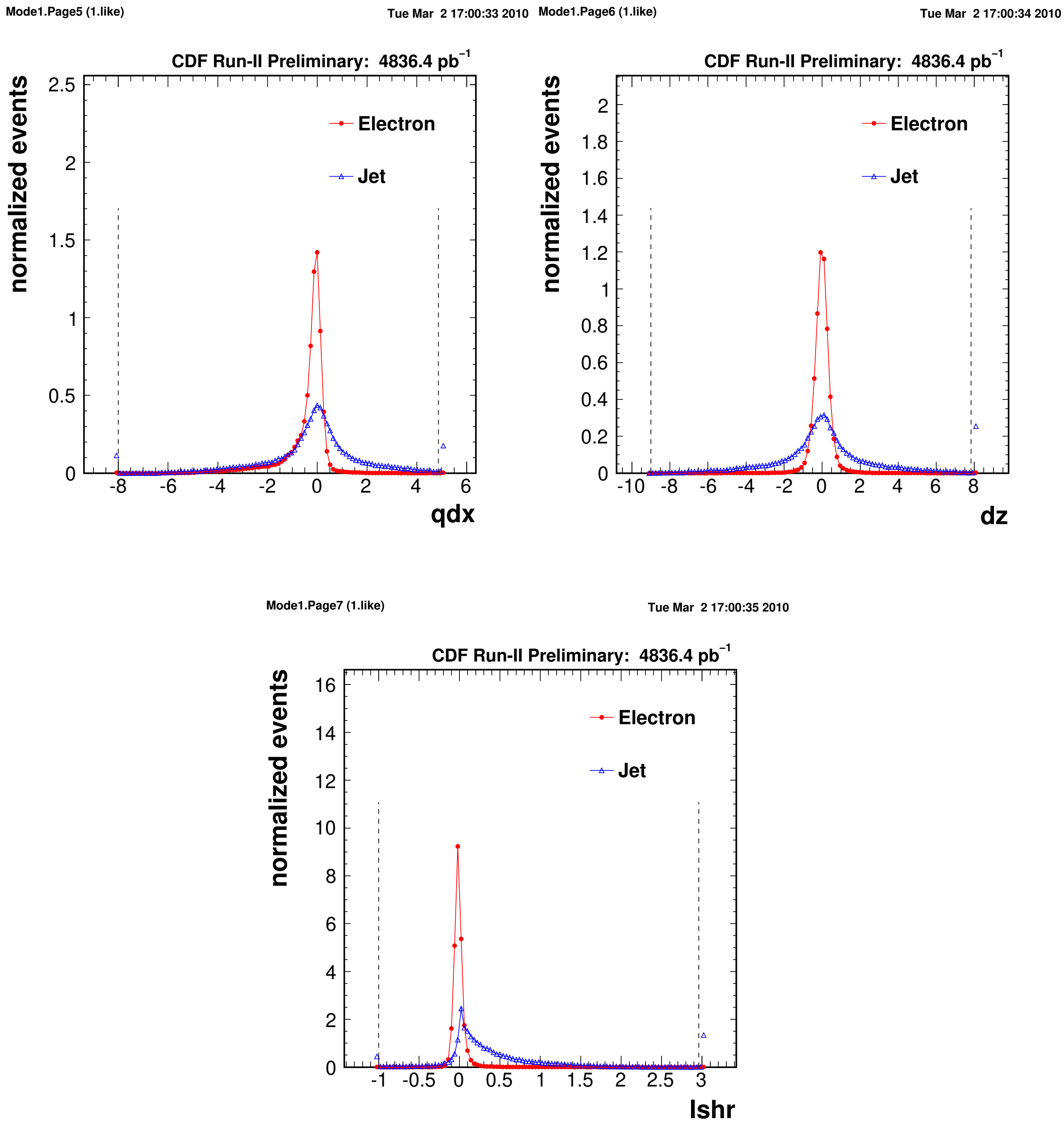

Figure 5: Normalized distributions of the identification variables for electrons from Z decays compared to those for electron candidates in jet samples.

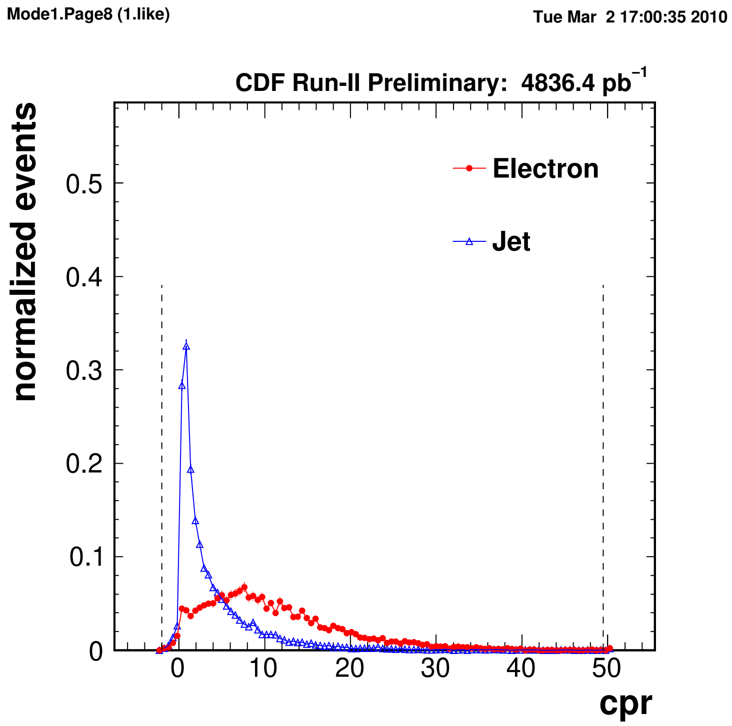

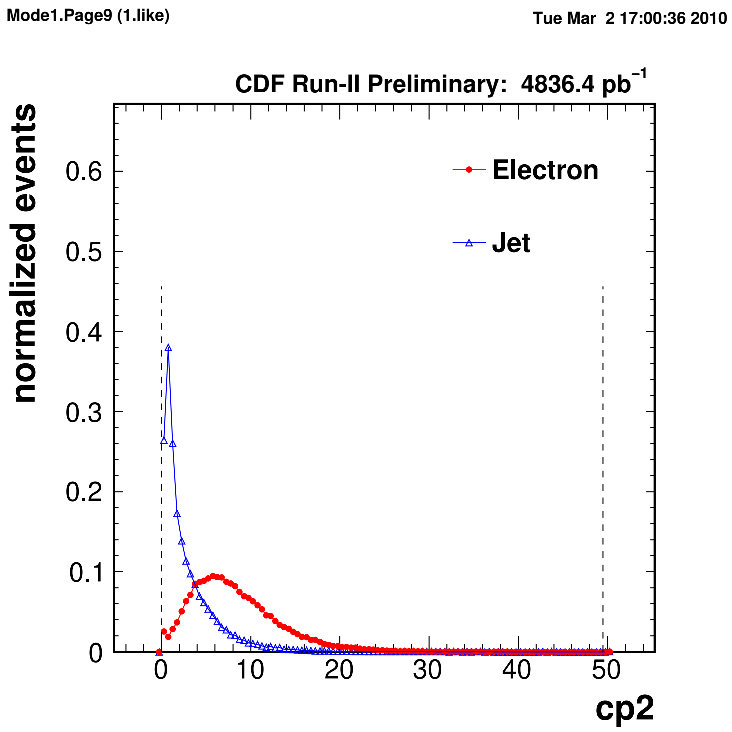

Figure 6: Normalized distributions of the identification variables for electrons from Z decays compared to those for electron candidates in jet samples.

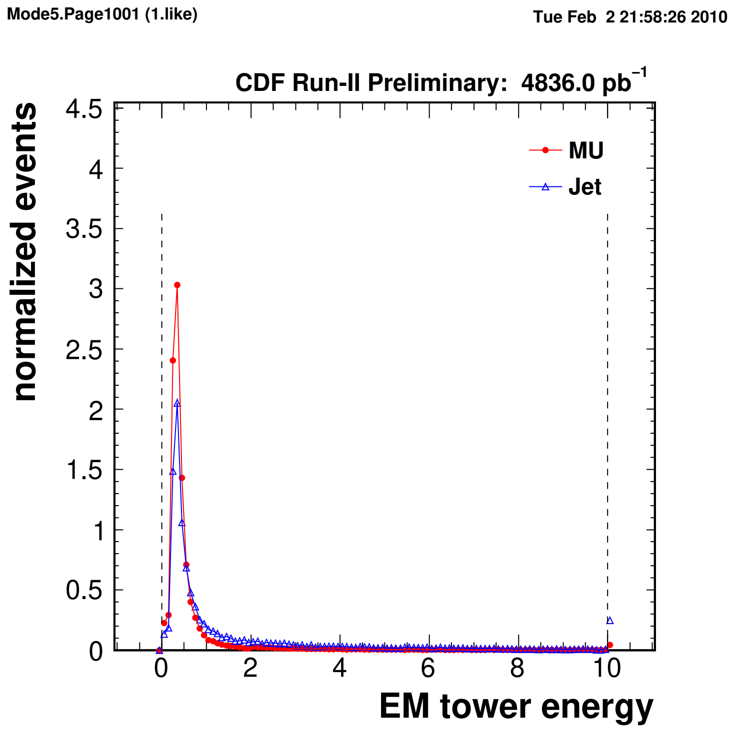

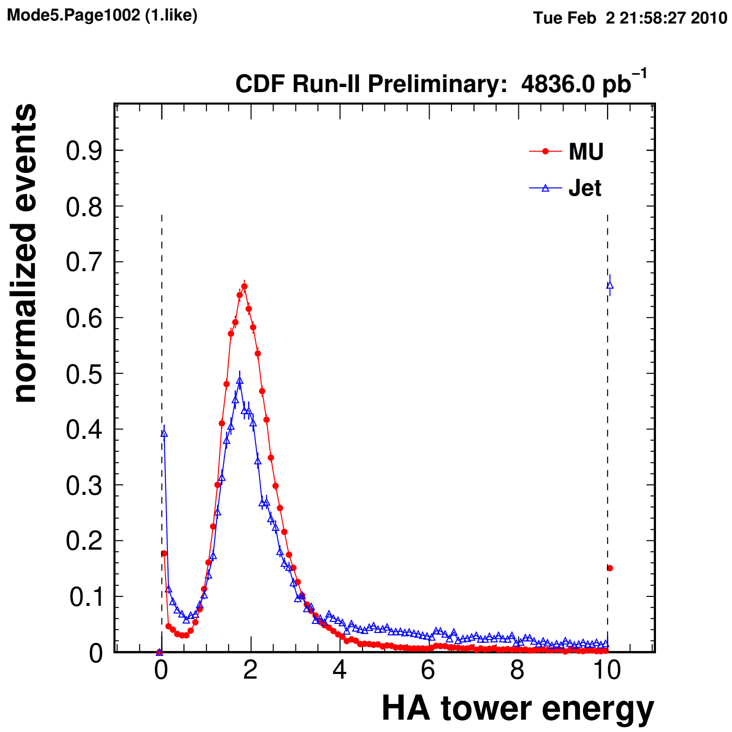

Figure 7: Normalized distributions of the identification variables for muons from Z decays compared to those for muon candidates in jet samples.

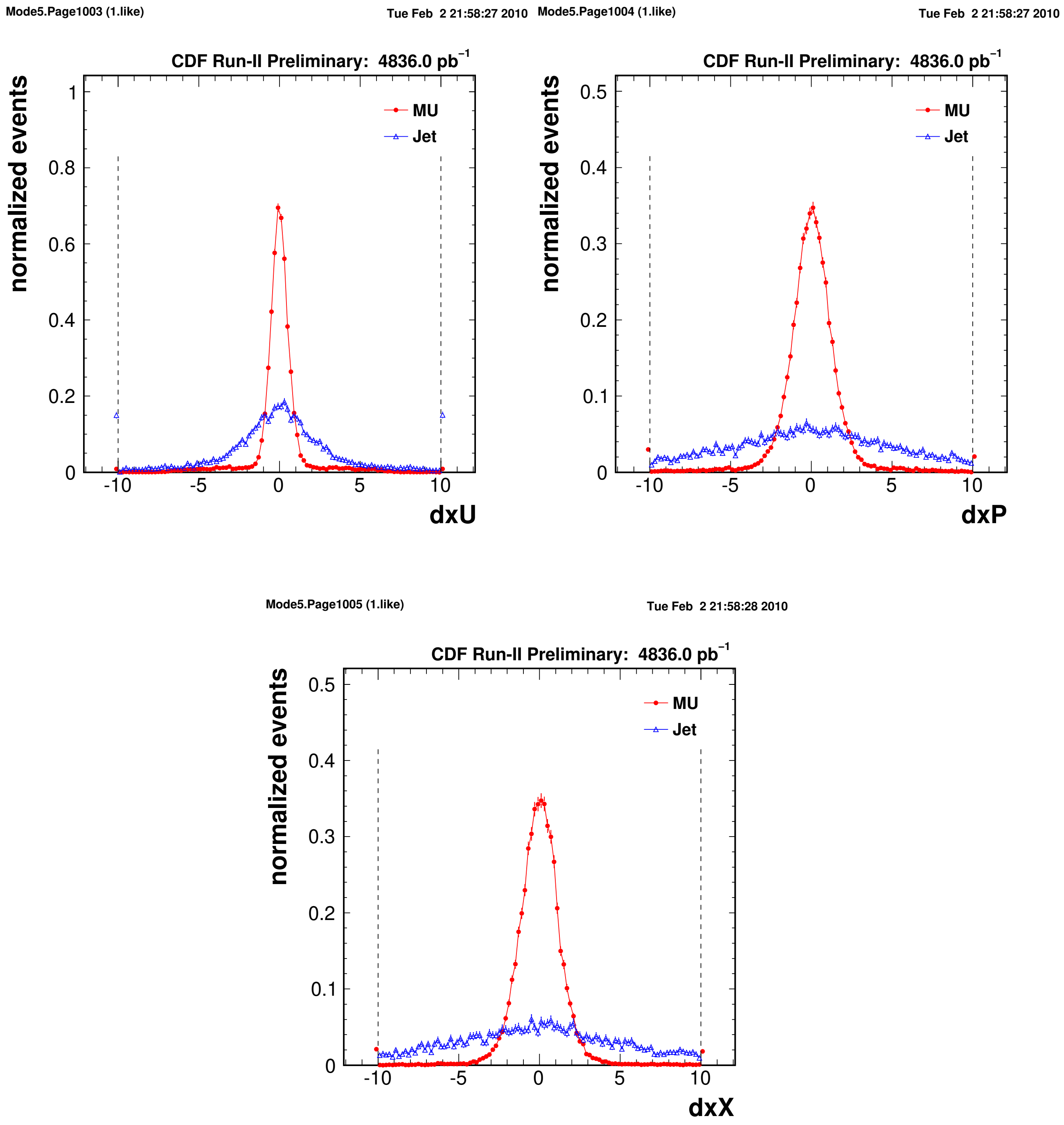

Figure 8: Normalized distributions of the identification variables for muons from Z decays compared to those for muon candidates in jet samples.

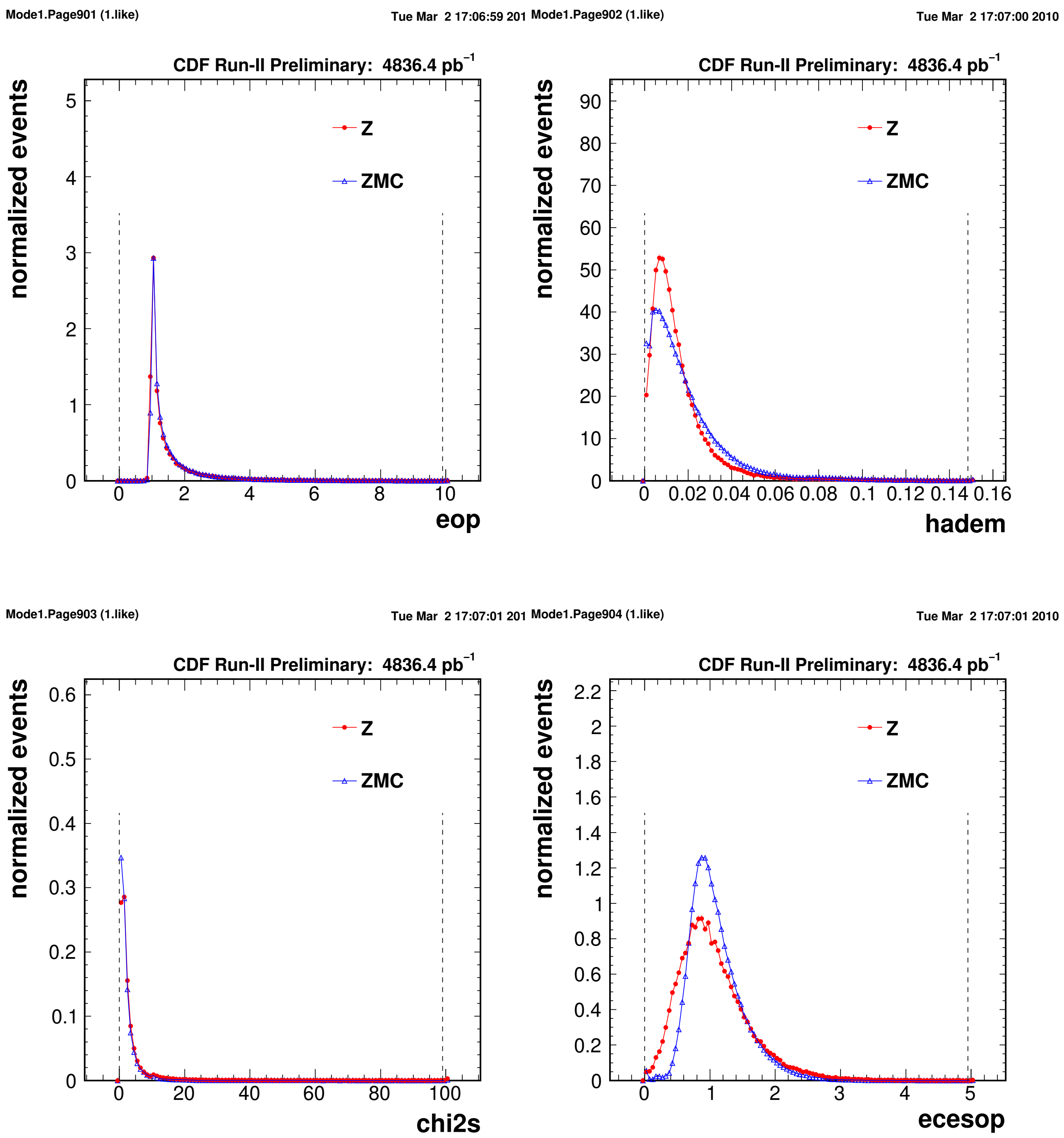

Figure 9: Normalized distributions of the identification variables for electrons from Z decays compared to those for electrons in Z Monte Carlo data.

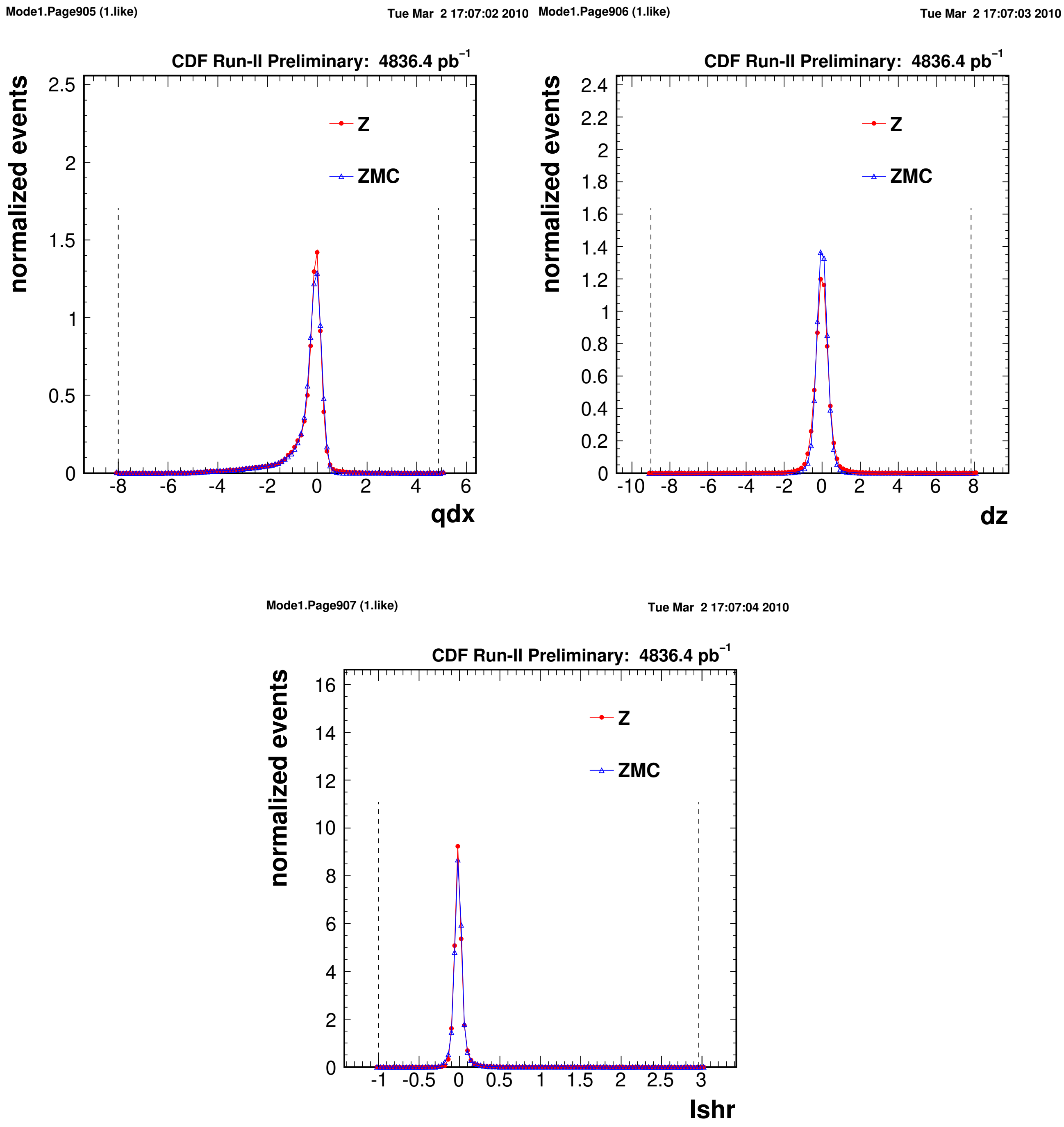

Figure 10: Normalized distributions of the identification variables for electrons from Z decays compared to those for electrons in Z Monte Carlo data.

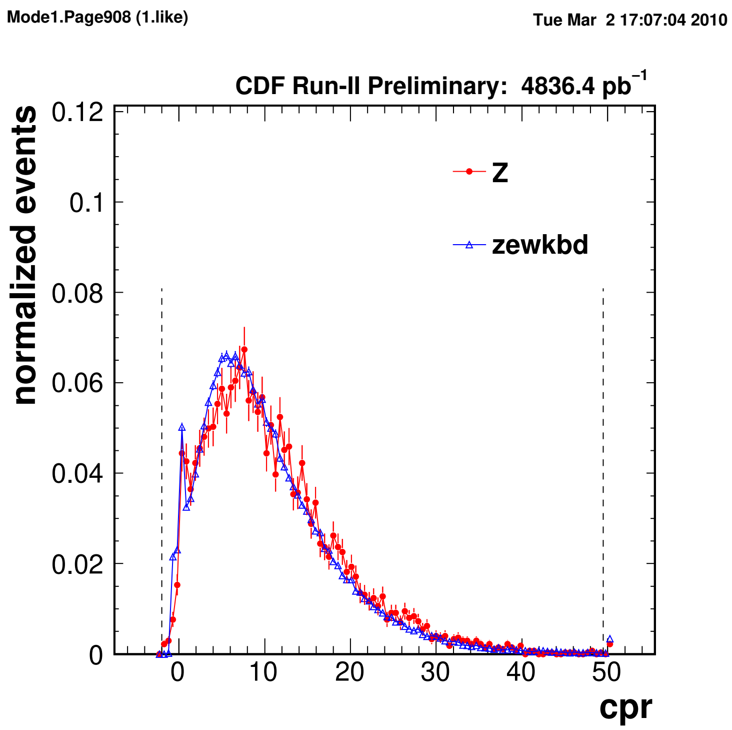

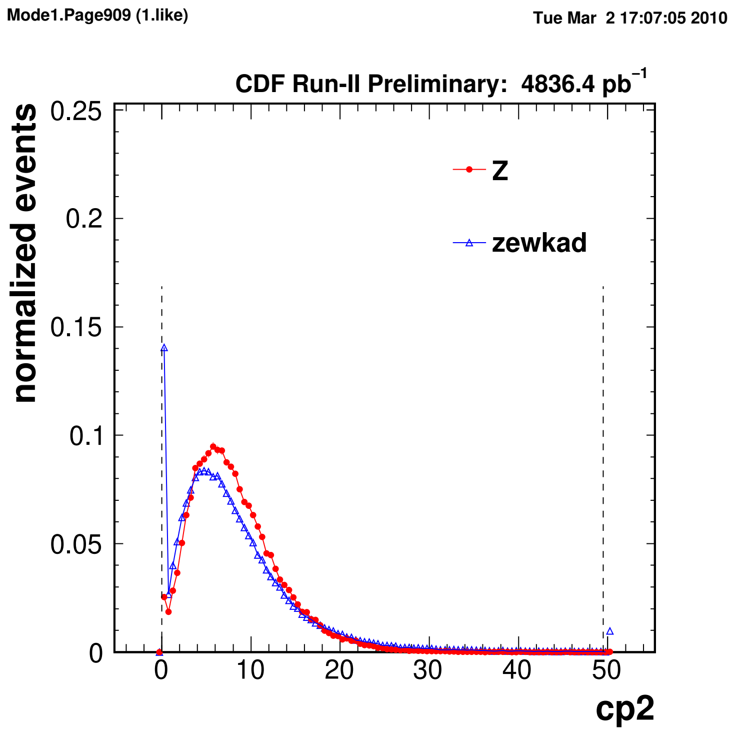

Figure 11: Normalized distributions of the identification variables for electrons from Z decays compared to those for electrons in Z Monte Carlo data.

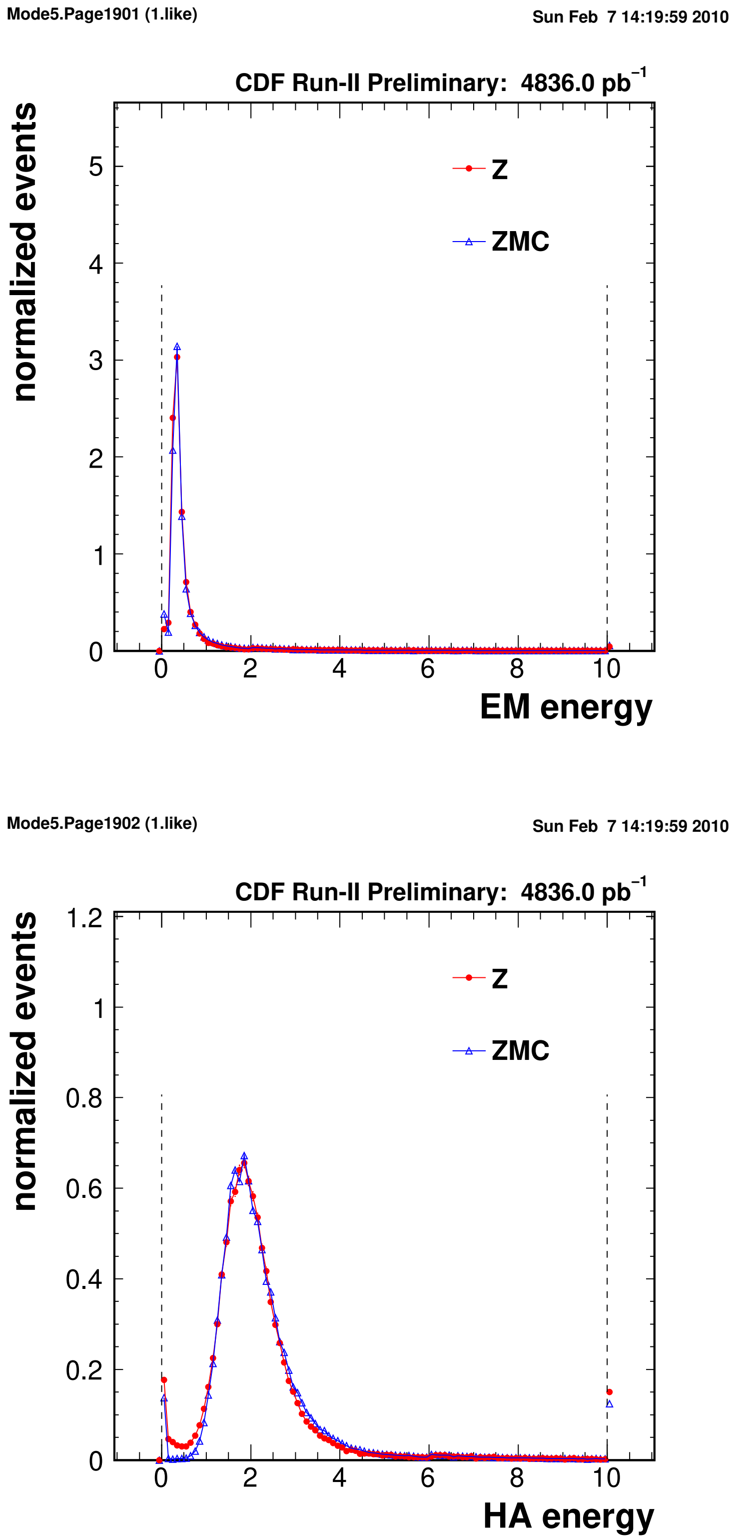

Figure 12: Normalized distributions of the identification variables for muons from Z decays compared to those for muons in Z Monte Carlo data.

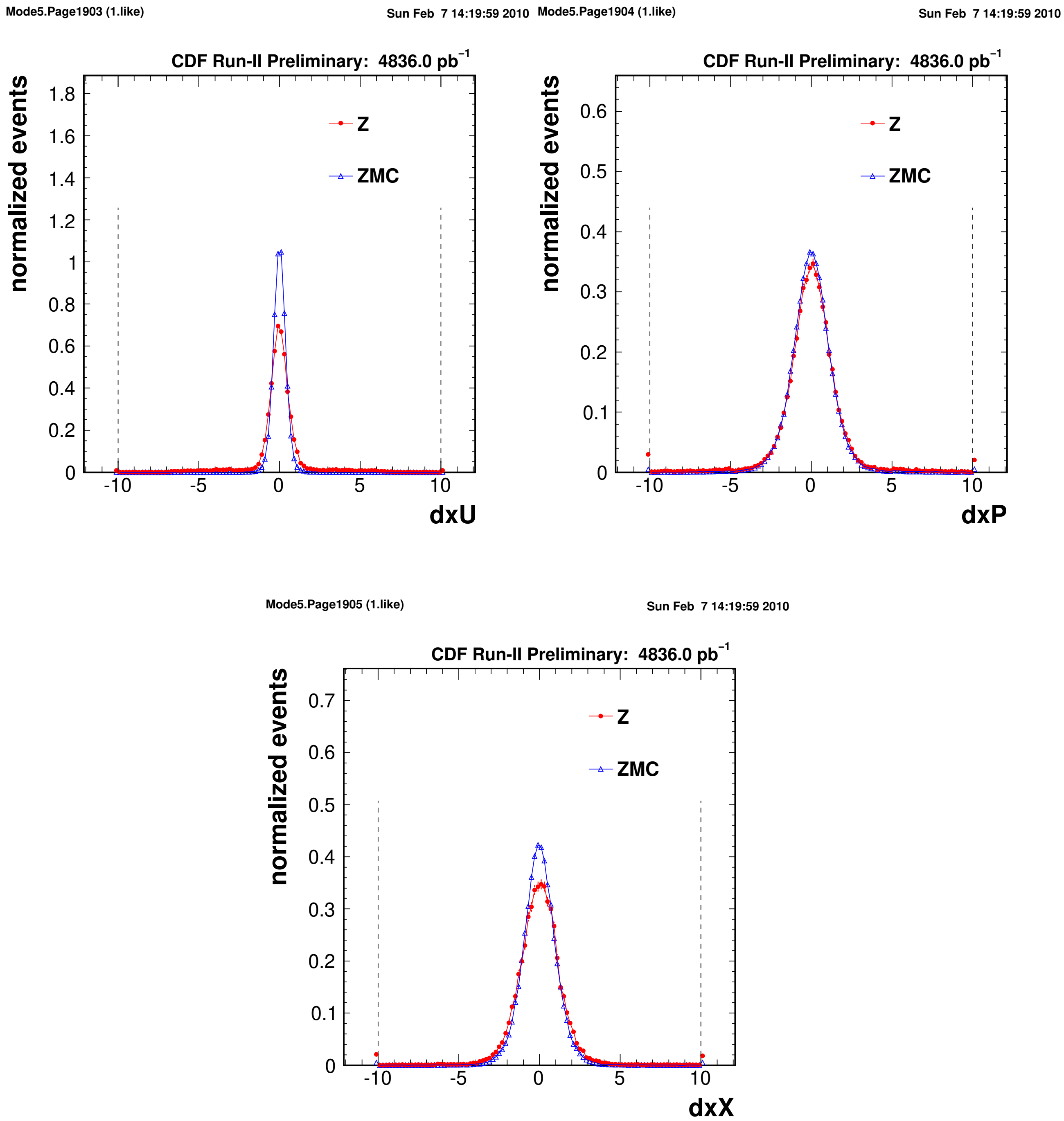

Figure 13: Normalized distributions of the identification variables for muons from Z decays compared to those for muons in Z Monte Carlo data.

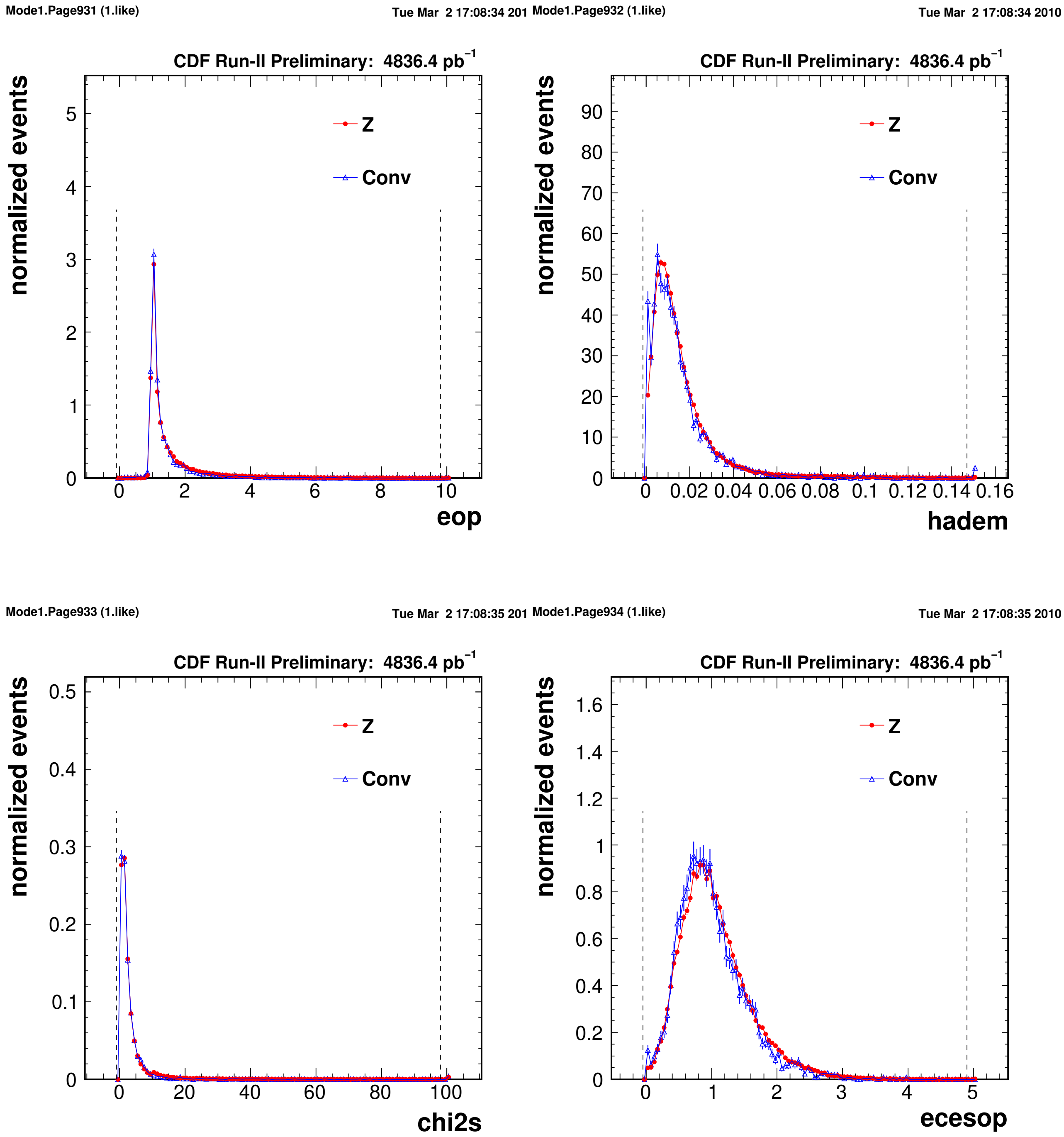

Figure 14: Normalized distributions of the identification variables for electrons from Z decays compared to those for conversion electrons.

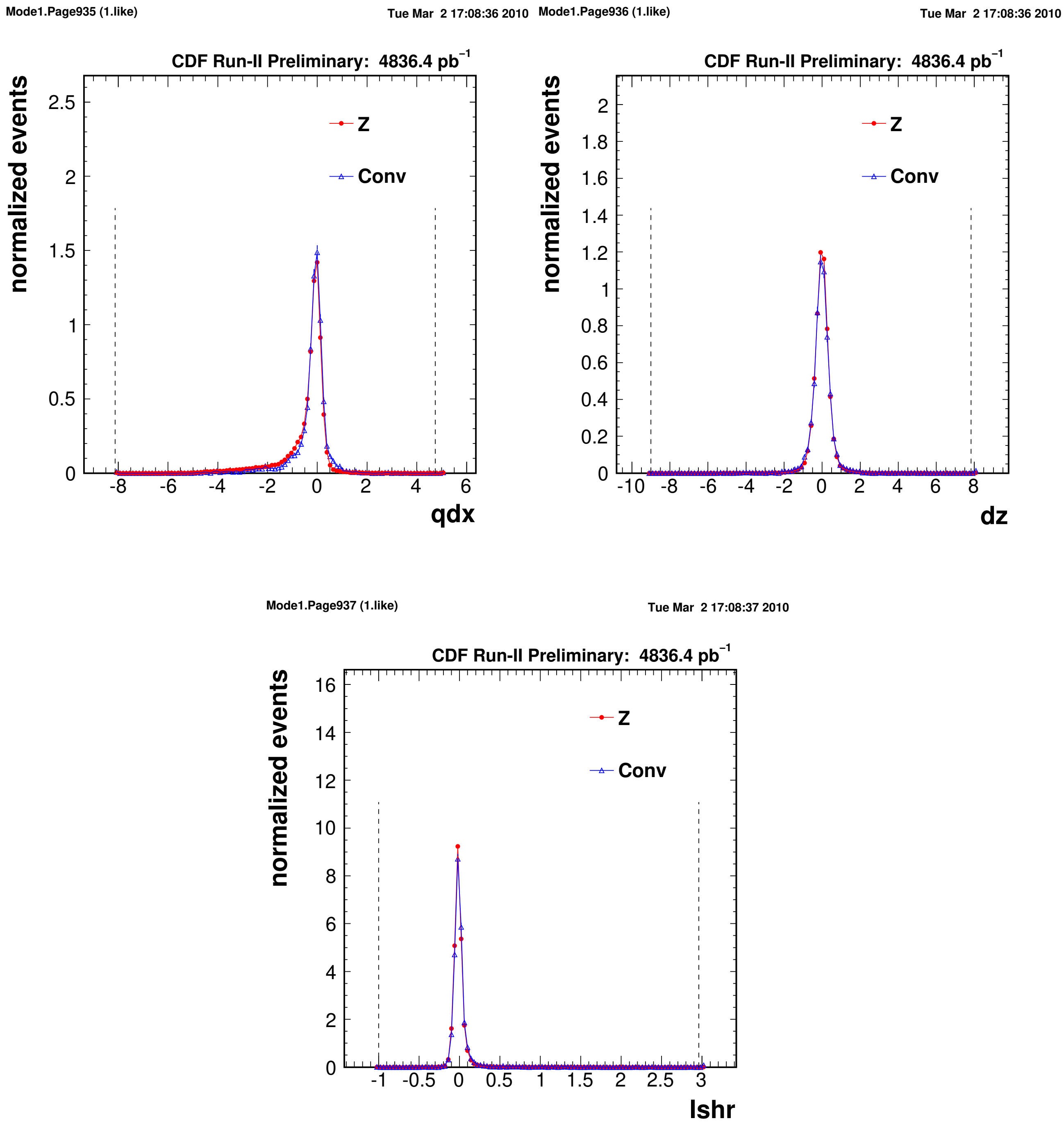

Figure 15: Normalized distributions of the identification variables for electrons from Z decays compared to those for conversion electrons.

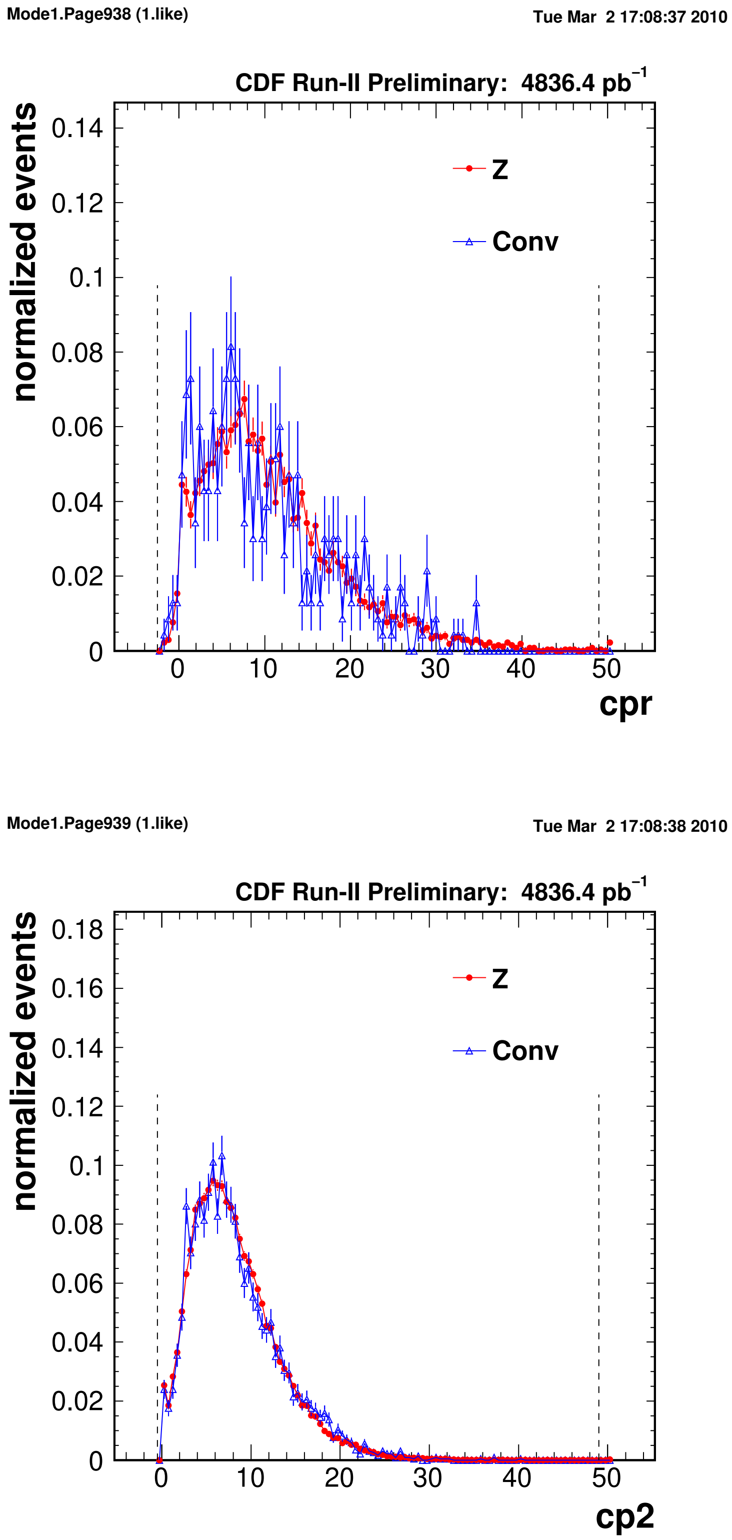

Figure 16: Normalized distributions of the identification variables for electrons from Z decays compared to those for conversion electrons.

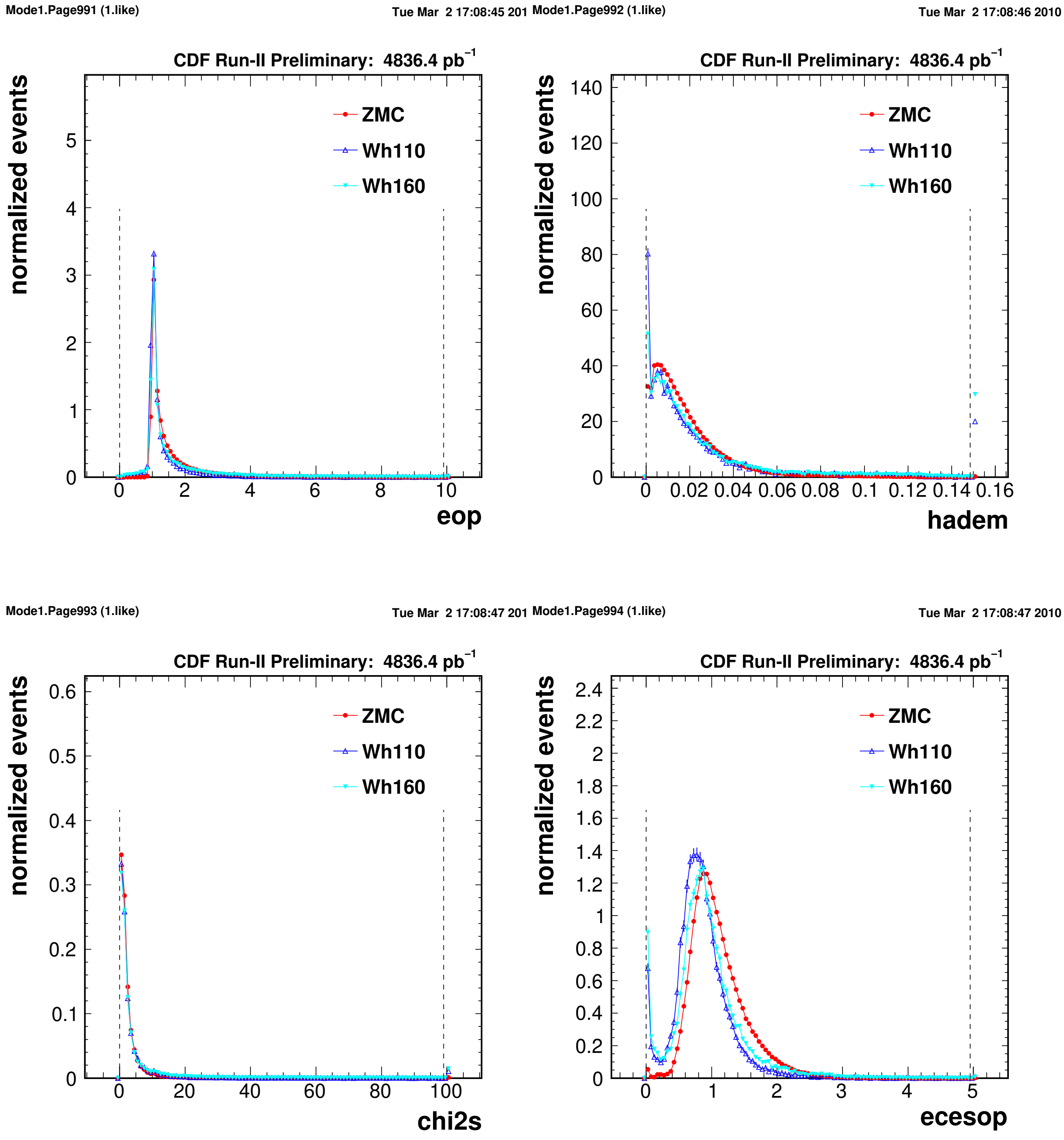

Figure 17: Comparisons of normalized distributions of electron identification variables among three Monte Carlo samples: Z, higgs with the mass 110 GeV/c^2, and 160 GeV/c^2.

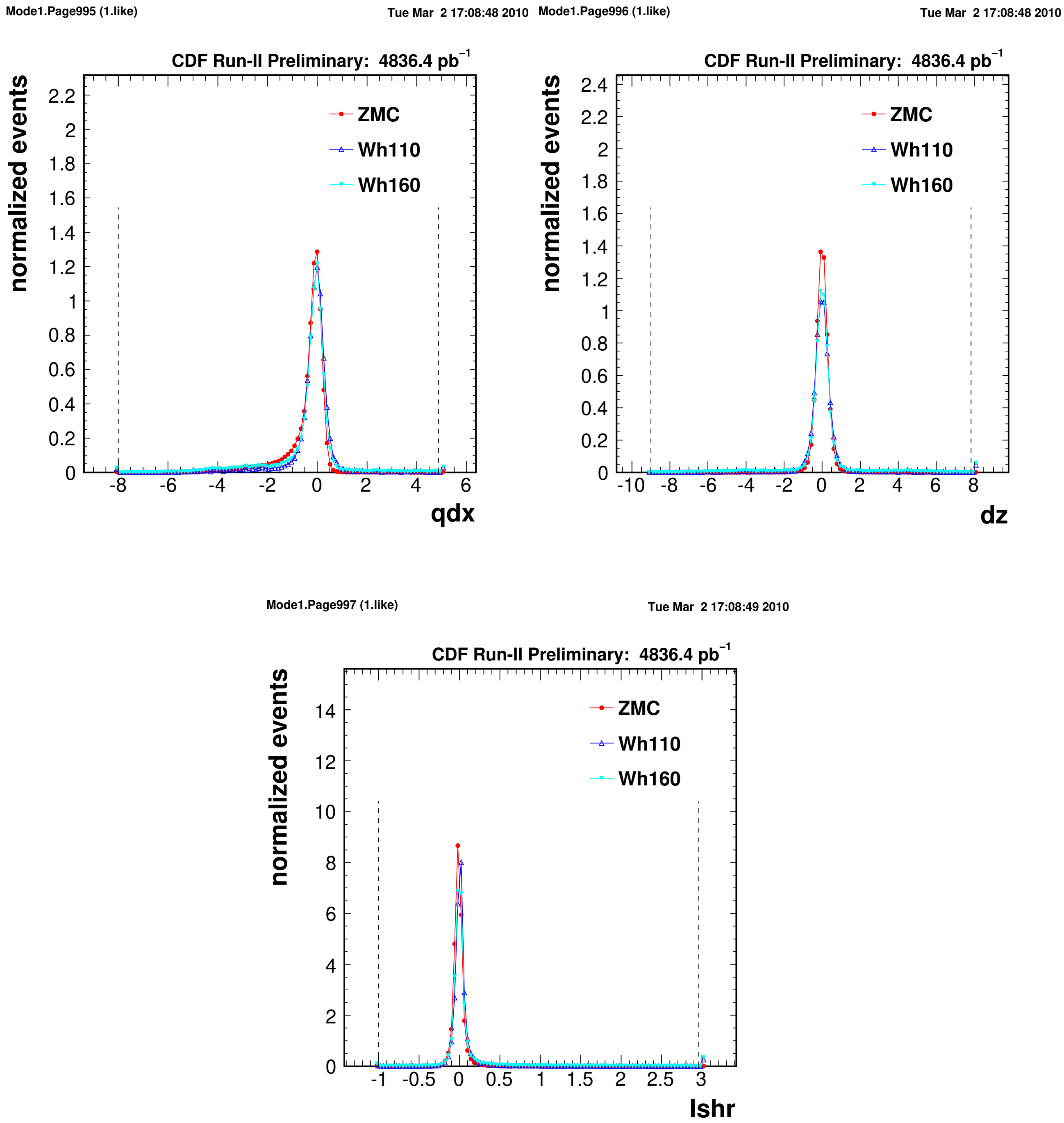

Figure 18: Comparisons of normalized distributions of electron identification variables among three Monte Carlo samples: Z, higgs with the mass 110 GeV/c^2, and 160 GeV/c^2.

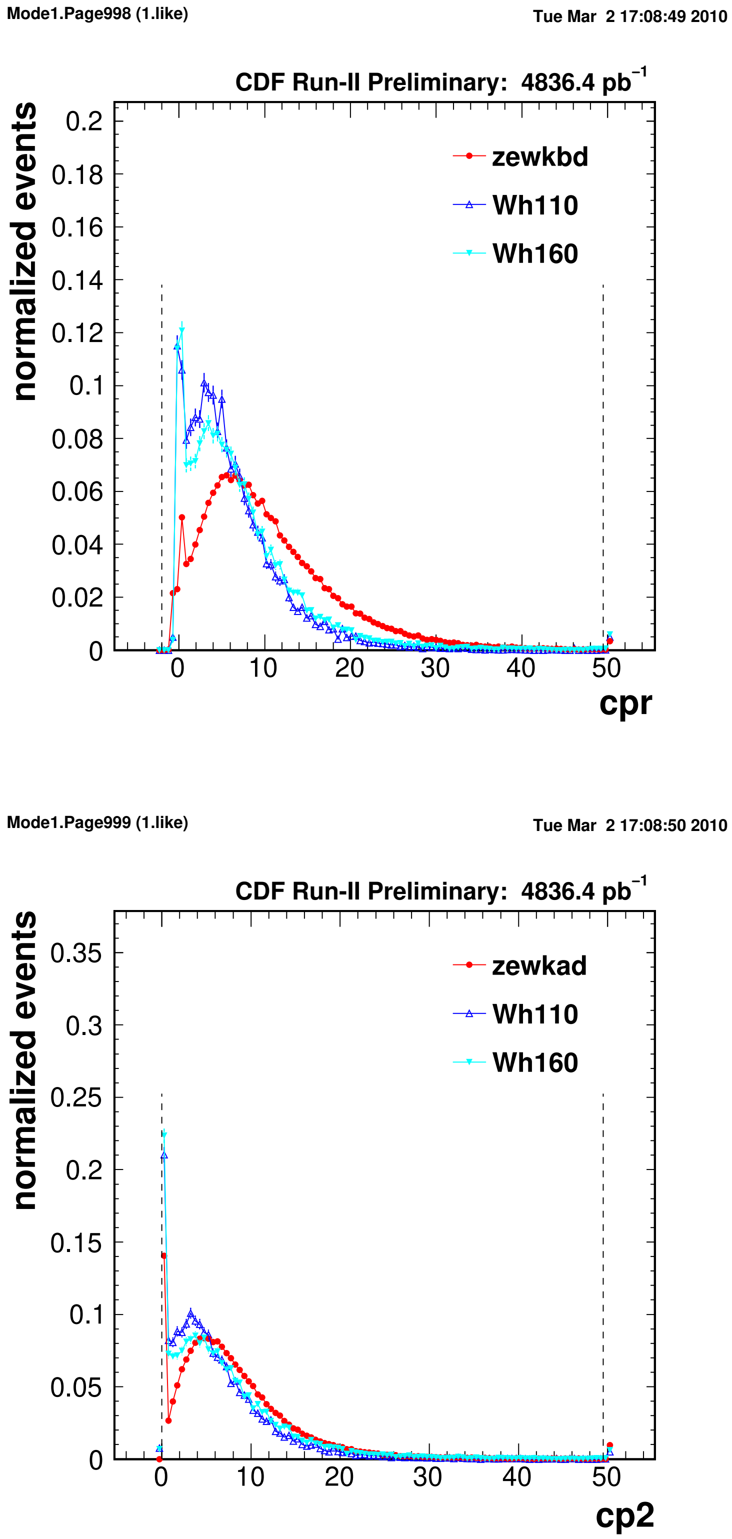

Figure 19: Comparisons of normalized distributions of electron identification variables among three Monte Carlo samples: Z, higgs with the mass 110 GeV/c^2, and 160 GeV/c^2.

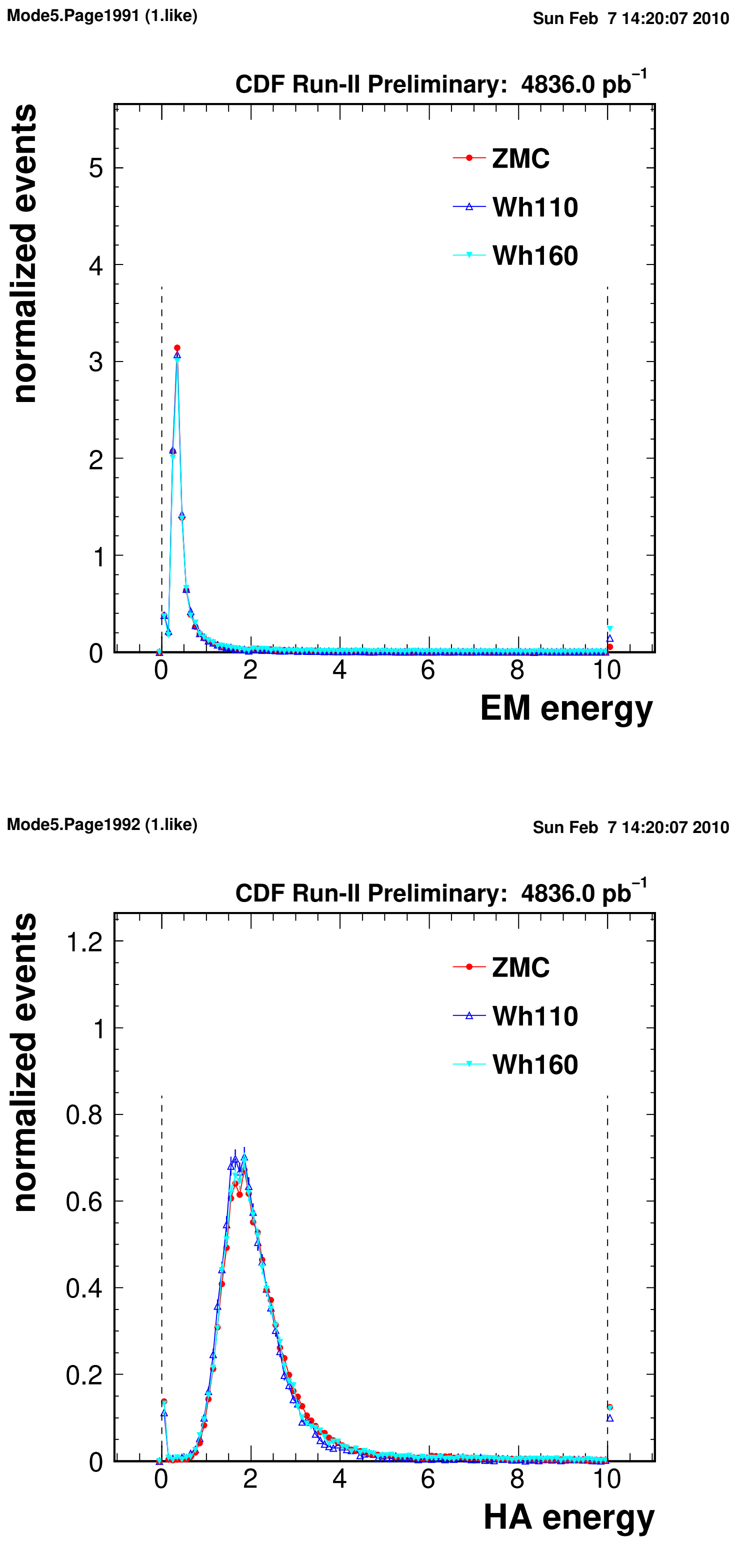

Figure 20: Comparisons of normalized distributions of muon identification variables among three Monte Carlo samples: Z, higgs with the mass 110 GeV/c^2, and 160 GeV/c^2.

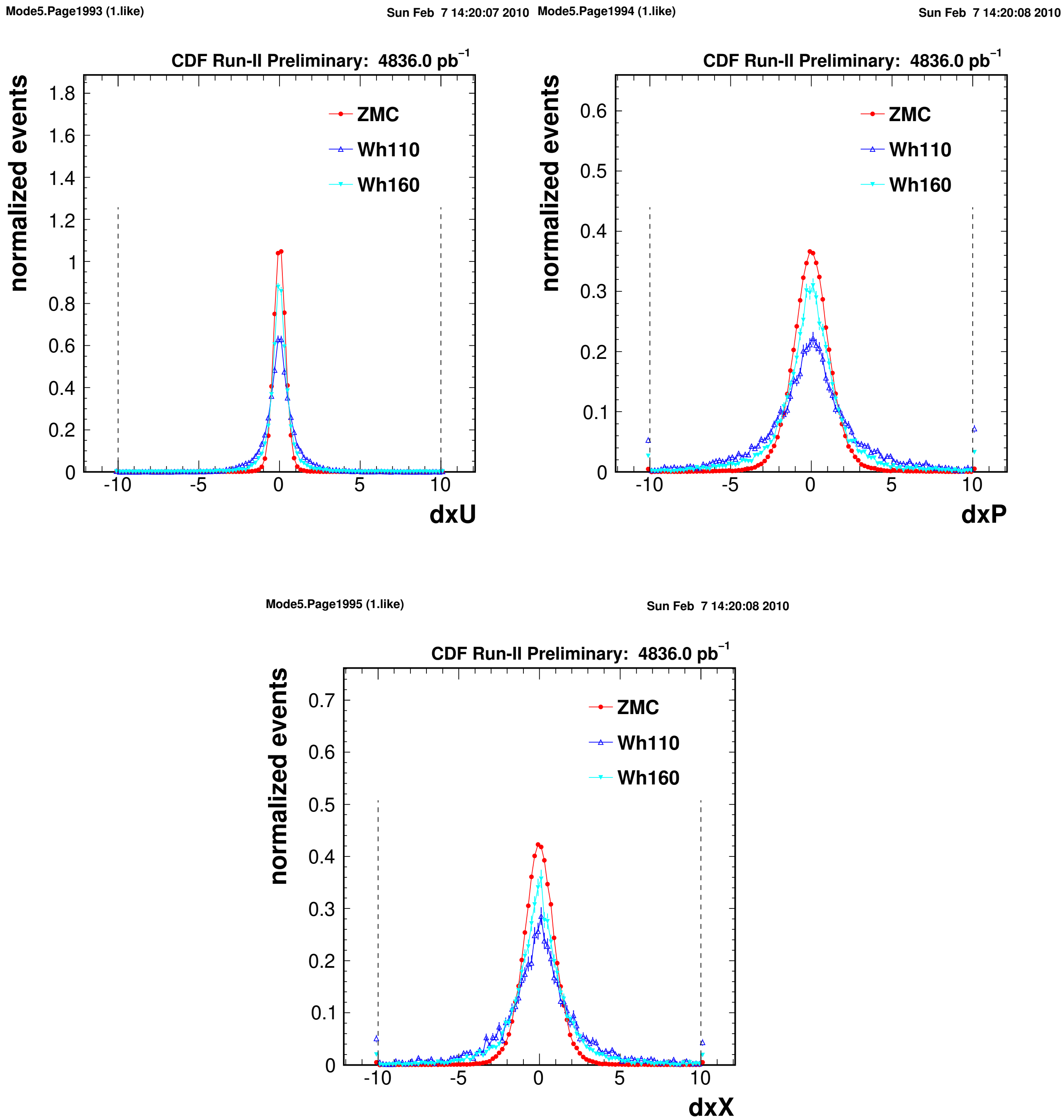

Figure 21: Comparisons of normalized distributions of muon identification variables among three Monte Carlo samples: Z, higgs with the mass 110 GeV/c^2, and 160 GeV/c^2.

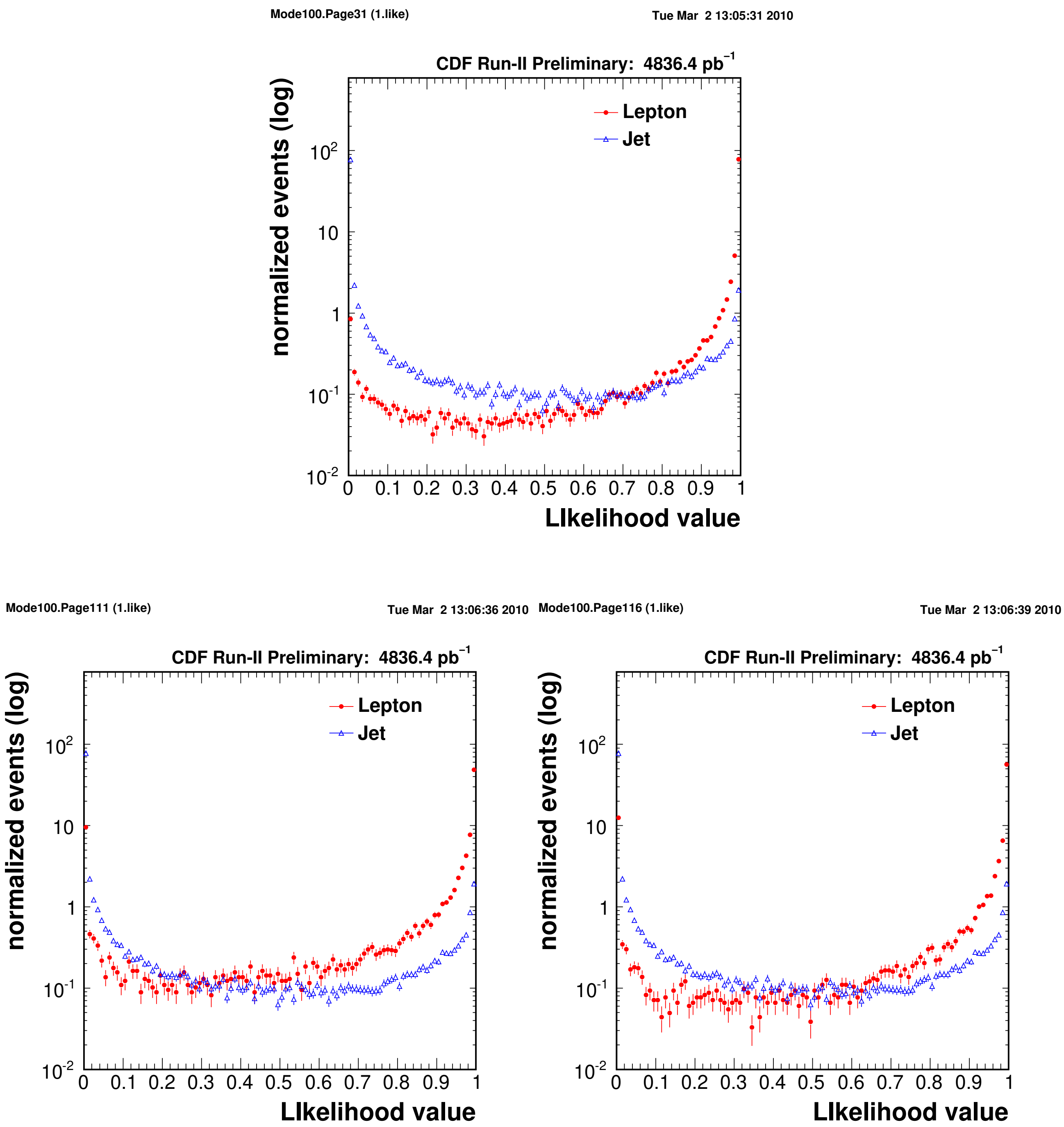

Figure 22: Likelihood distributions, after normalized, for electrons and fake electrons. The signal samples are Z events (top), higgs Monte Carlo with the mass 110 GeV/c^2 (bottom-left), and 160 GeV/c^2 (bottom-right), while the jet sample is the `Jet20`. The signal PDFs are created from Z electrons.

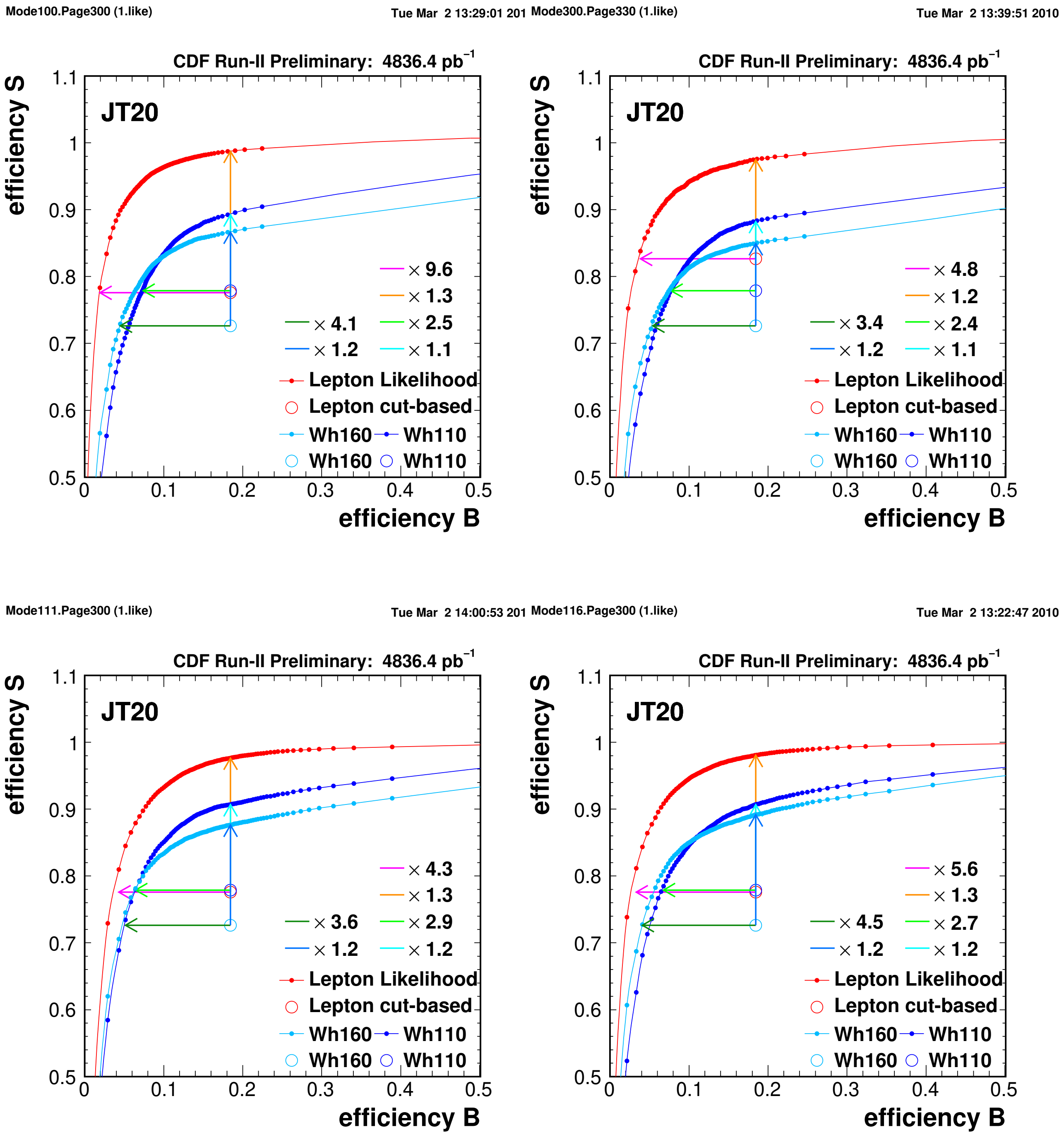

Figure 23: Signal efficiency as a function of background efficiency for the likelihood-based electron identification, where the signal samples are Z events, higgs Monte Carlo with the mass of 110 GeV/c^2, and 160 GeV/c^2, while the background sample is the `Jet20`. The signal PDFs used for the likelihood calculations are Z electrons (top left), conversions (top right), higgs Monte Carlo with the mass of 110 GeV/c^2 (bottom left), and higgs with 160 GeV/c^2 (bottom right). The open points corresponds to the cut-based efficiency. The signal efficiency improvements are indicated by the vertical arrows, while the horizontal arrows represent the background reduction.

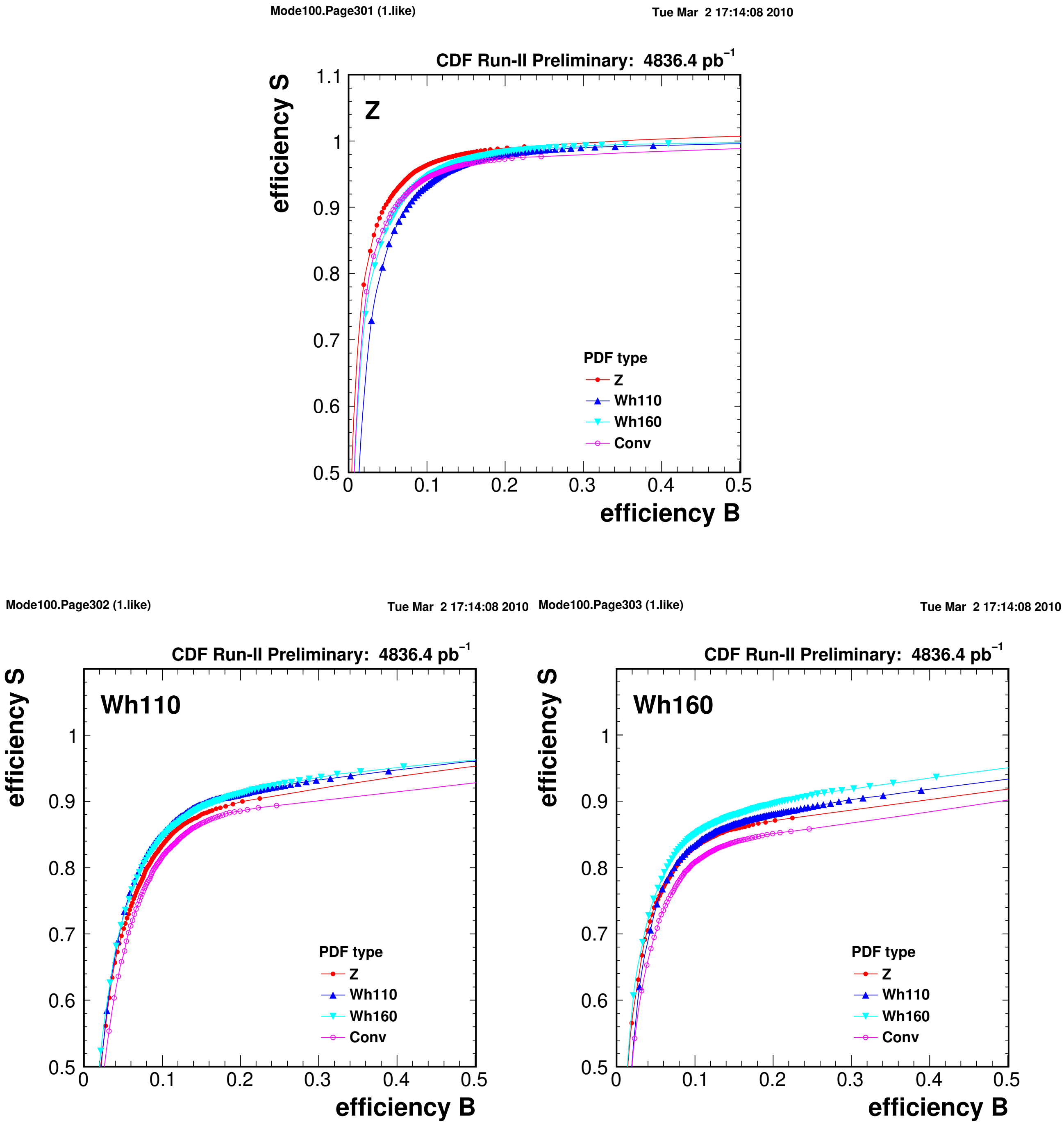

Figure 24: Signal efficiency as a function of background efficiency for the likelihood-based electron identification with comparing different kinds of signal PDFs for a given data sample.

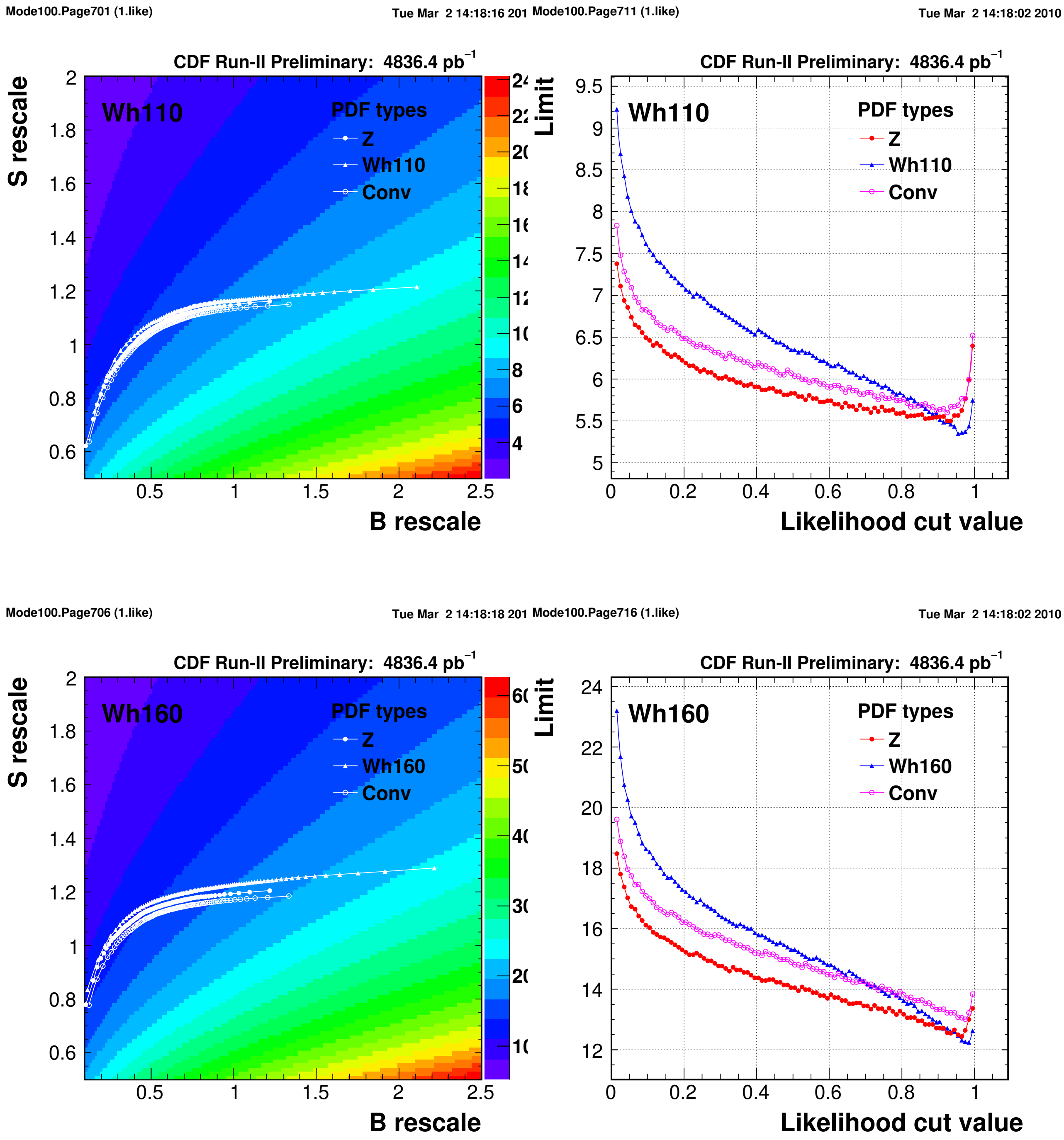

Figure 25: Limits on the signal vs. background plane superimposed with the efficiency curves of the likelihood-based electron identification (left) and limits as a function of likelihood cut-value (right). The results for the cut-based identification with rescaling the signal and background rates are used to map the limit on the signal vs. background plane. Each plot shows the results for three types of signal PDFs. The higgs masses are 110 GeV/c^2 (top) and 160 GeV/c^2 (bottom). The background sample is the `Jet20`.

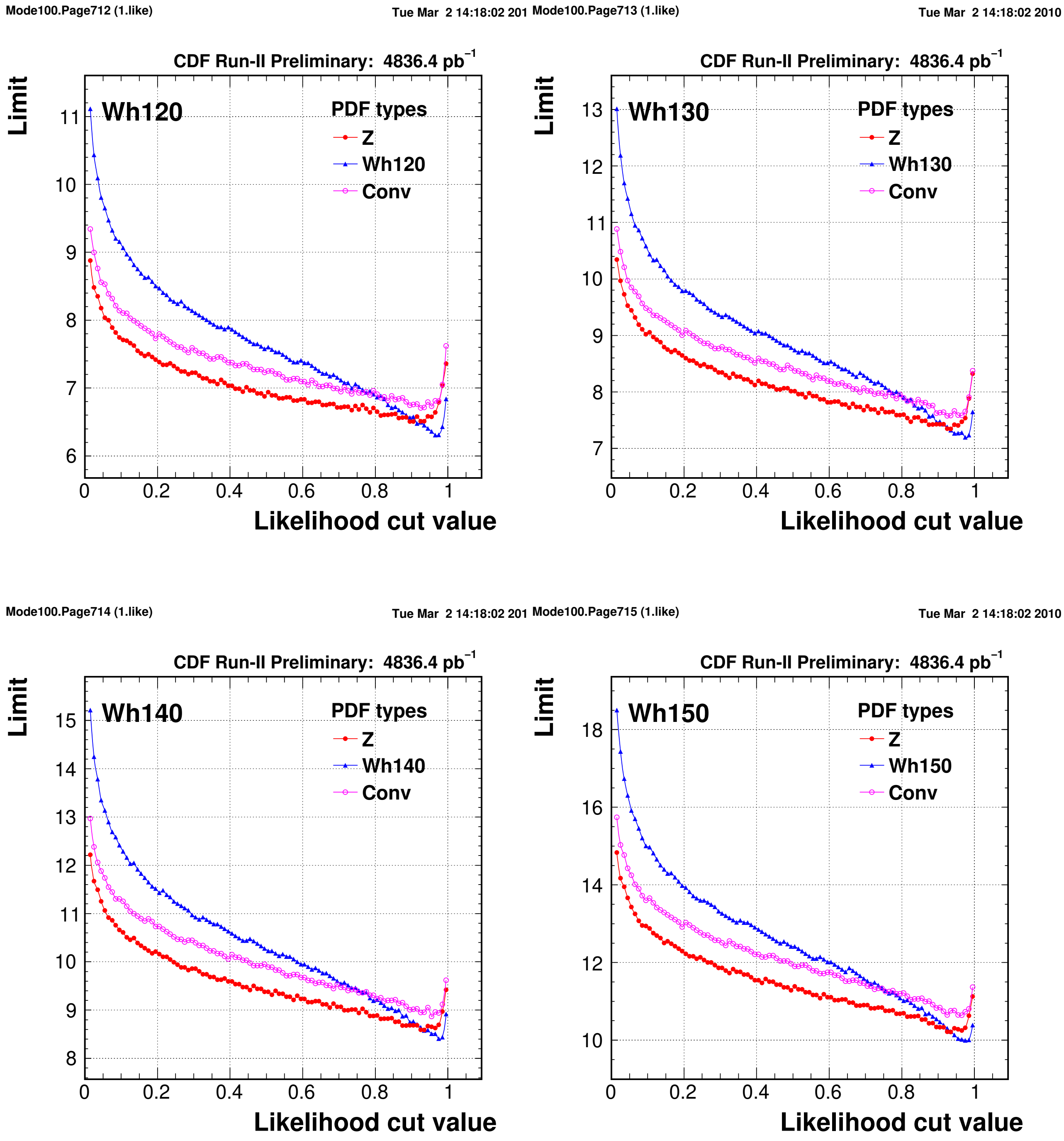

Figure 26: Limits as a function of electron-likelihood cut-value for three types of signal PDFs and for different higgs masses. The background sample is the `Jet20`.

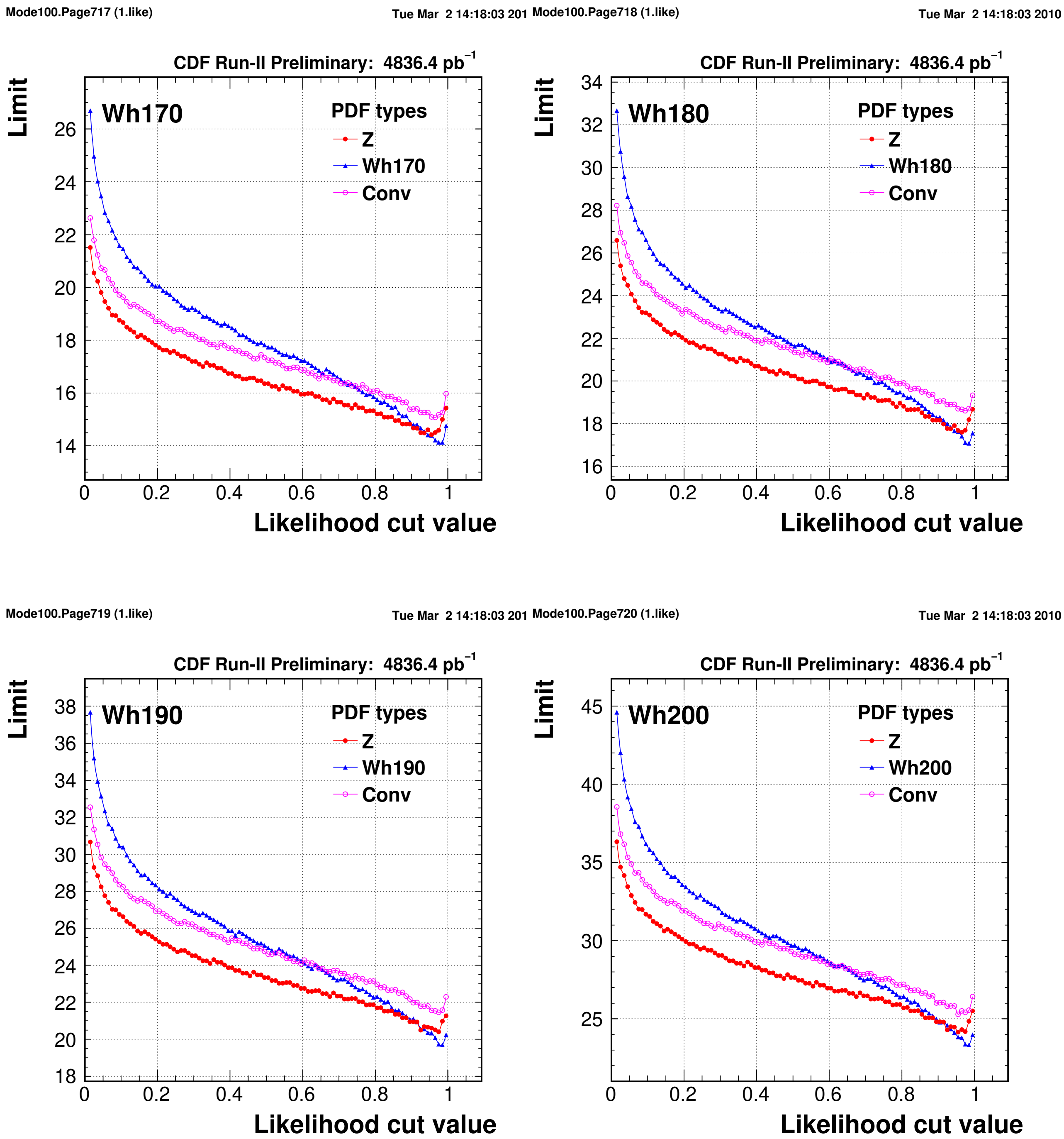

Figure 27: Limits as a function of electron-likelihood cut-value for three types of signal PDFs and for different higgs masses. The background sample is the `Jet20`.

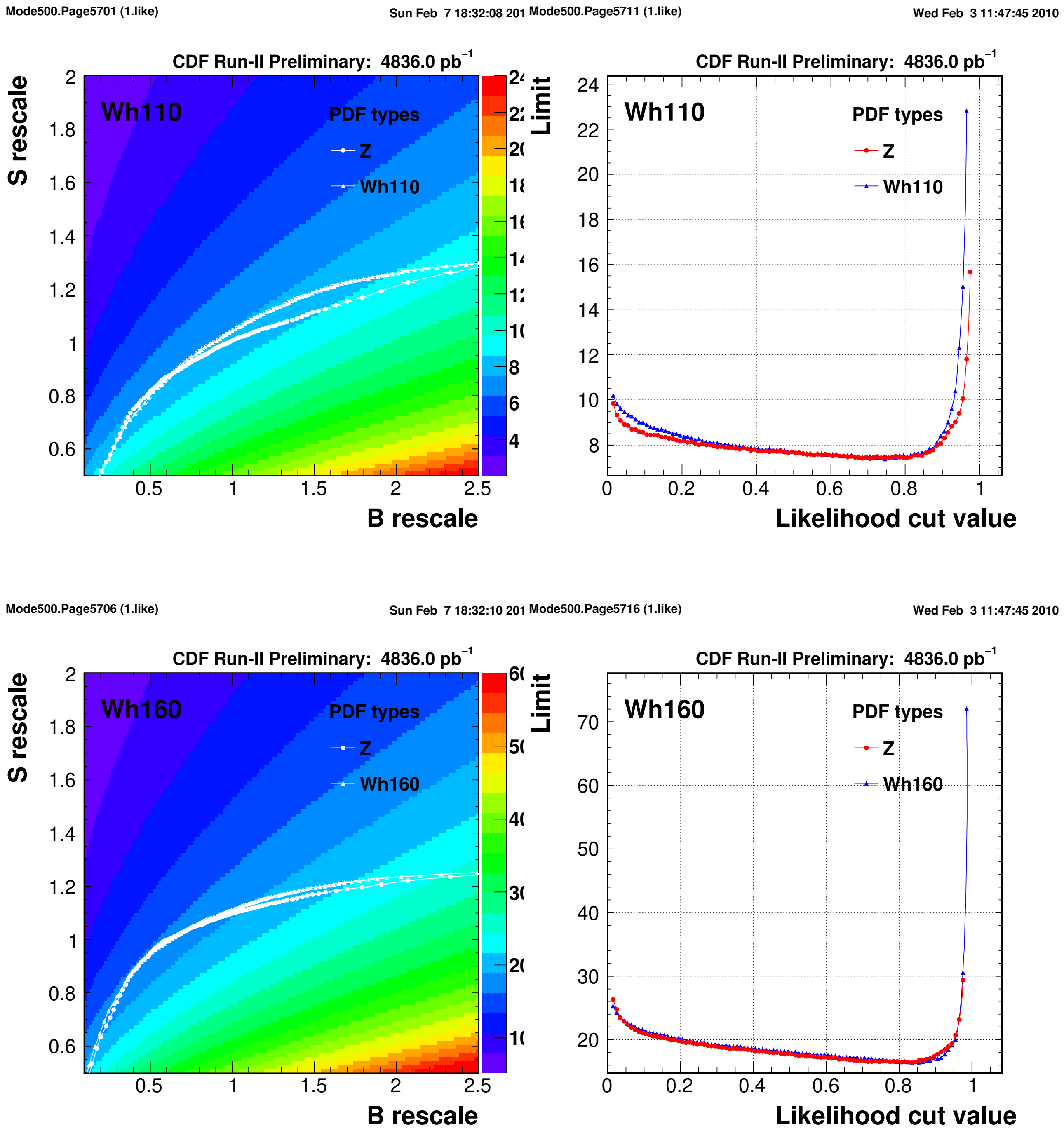

Figure 28: Limits on the signal vs. background plane superimposed with the efficiency curves of the likelihood-based CMUP muon identification (left) and limits as a function of likelihood cut-value (right). The results for the cut-based identification with rescaling the signal and background rates are used to map the limit on the signal vs. background plane. Each plot shows the results for three types of signal PDFs. The higgs masses are 110 GeV/c^2 (top) and 160 GeV/c^2 (bottom). The background sample is the `Jet20`.

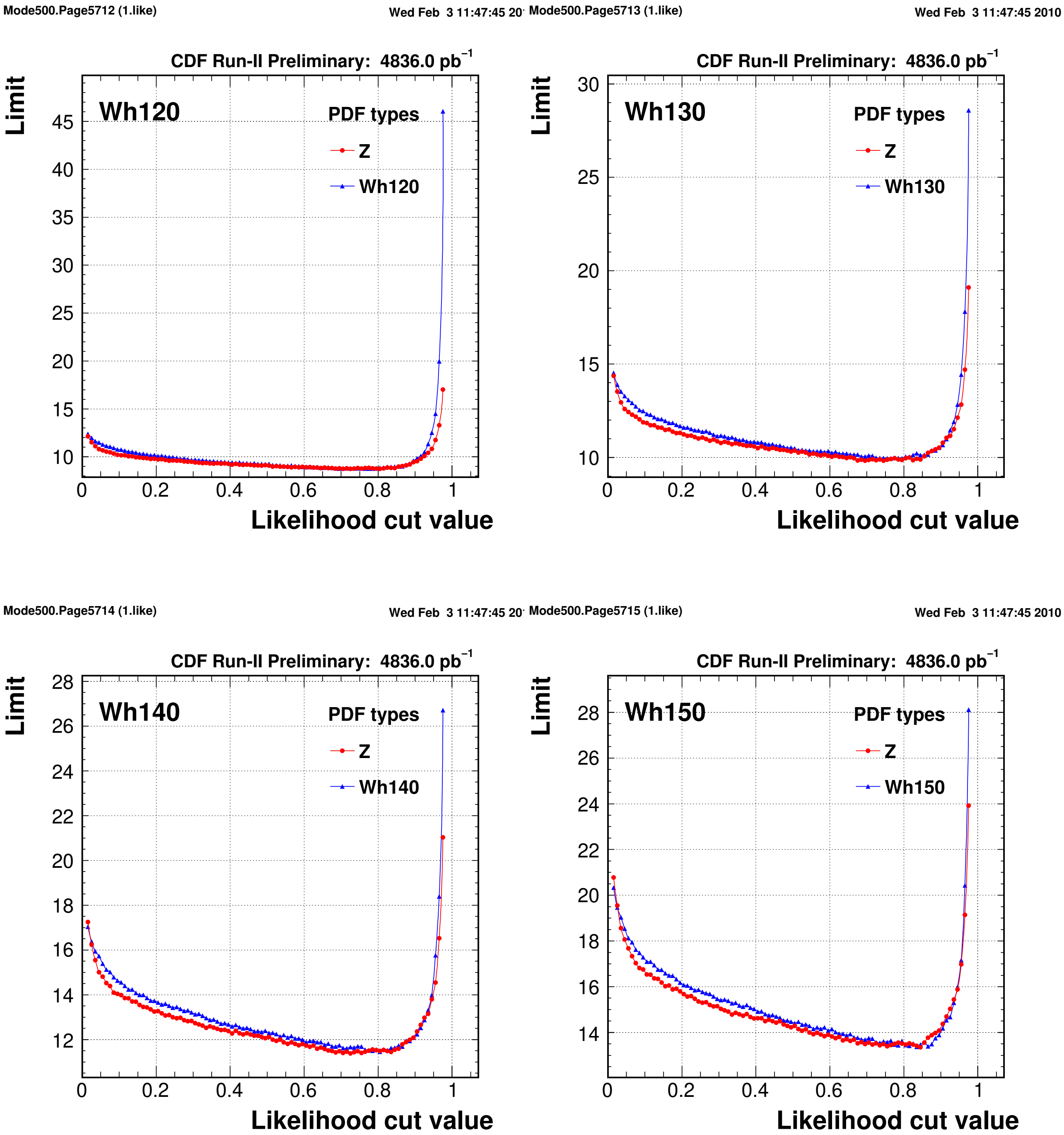

Figure 29: Limits as a function of CMUP-likelihood cut-value for three types of signal PDFs and for different higgs masses. The background sample is the `Jet20`.

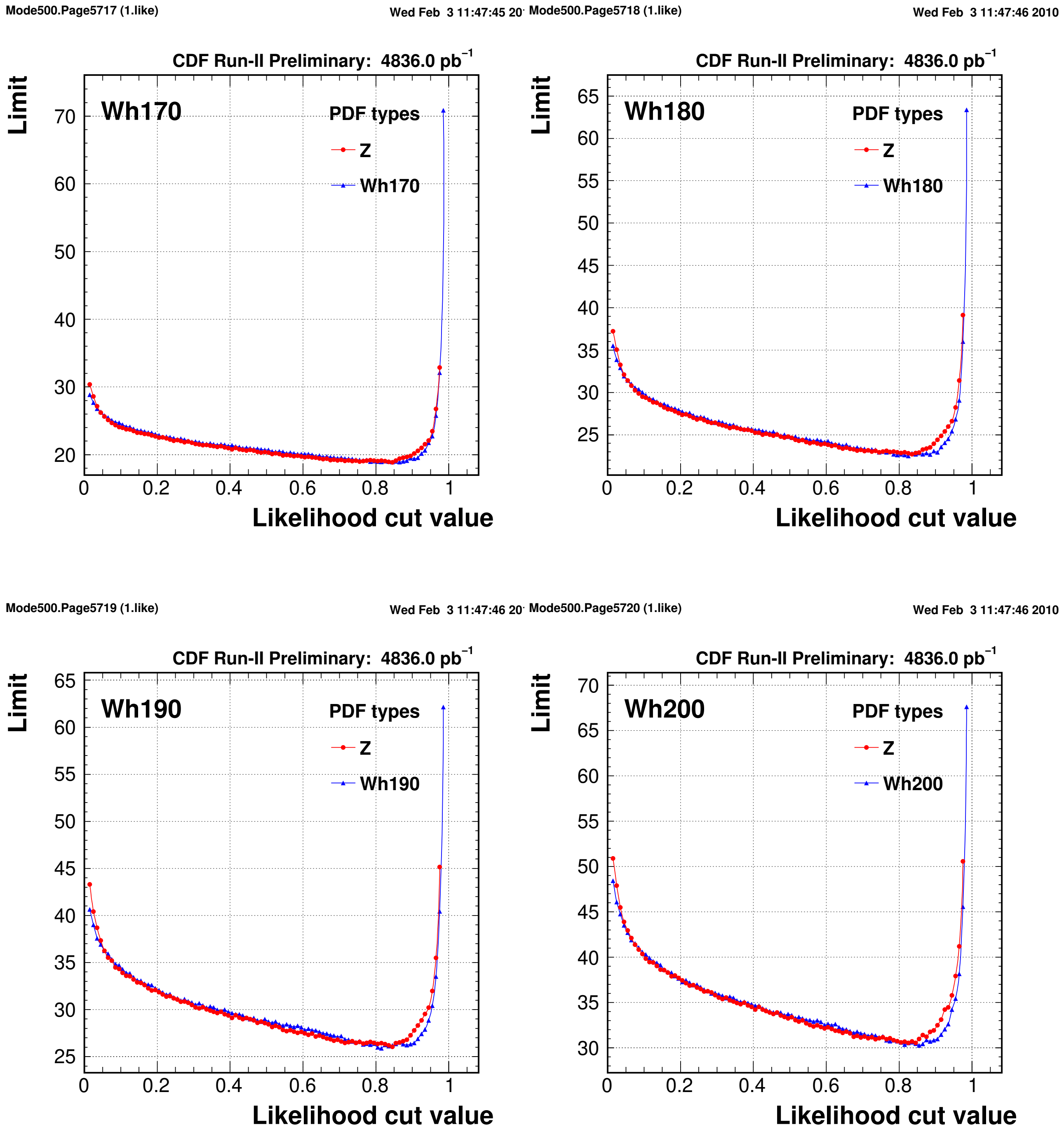

Figure 30: Limits as a function of CMUP-likelihood cut-value for three types of signal PDFs and for different higgs masses. The background sample is the `Jet20`.

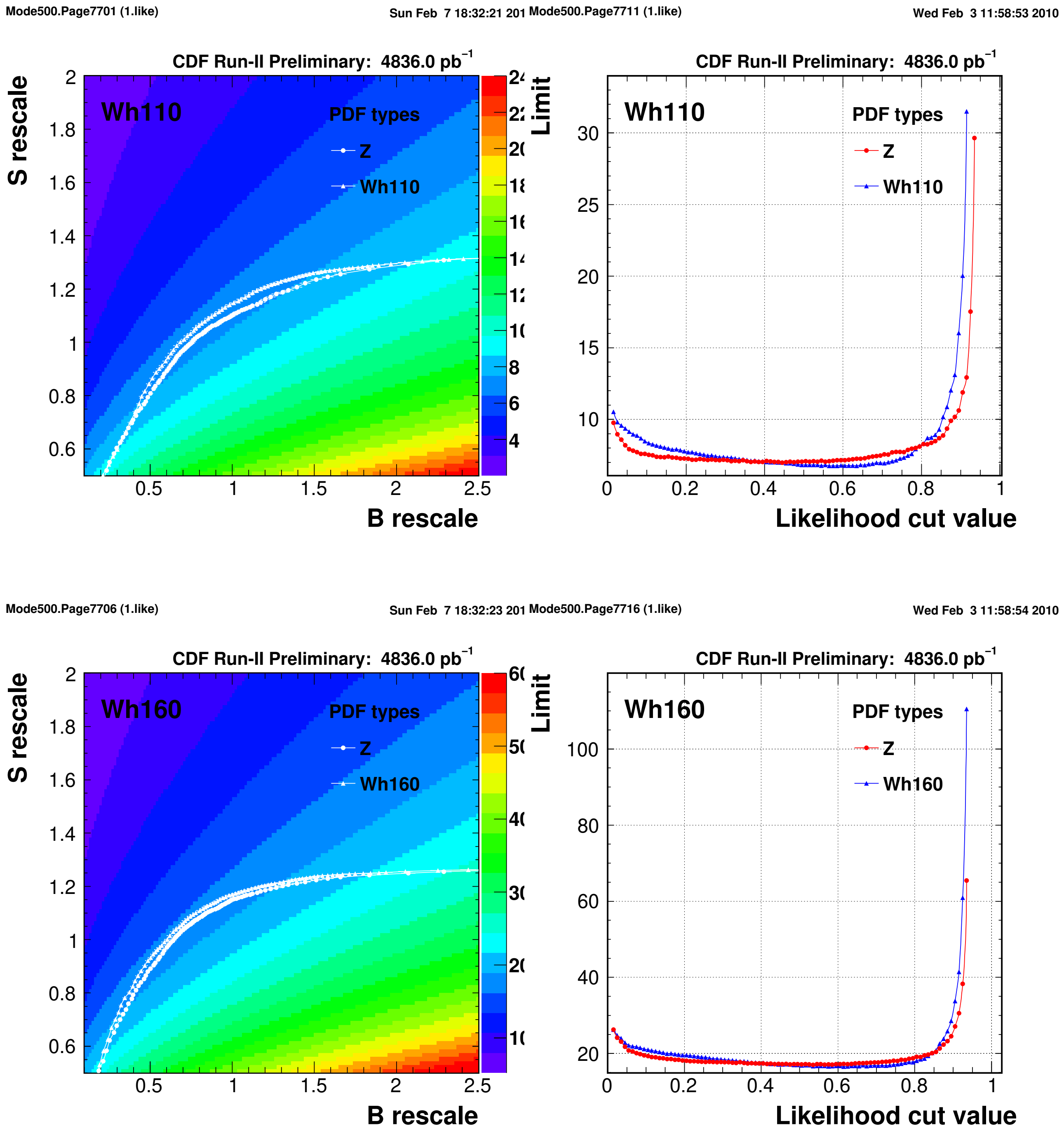

Figure 31: Limits on the signal vs. background plane superimposed with the efficiency curves of the likelihood-based CMX muon identification (left) and limits as a function of likelihood cut-value (right). The results for the cut-based identification with rescaling the signal and background rates are used to map the limit on the signal vs. background plane. Each plot shows the results for three types of signal PDFs. The higgs masses are 110 GeV/c^2 (top) and 160 GeV/c^2 (bottom). The background sample is the `Jet20`.

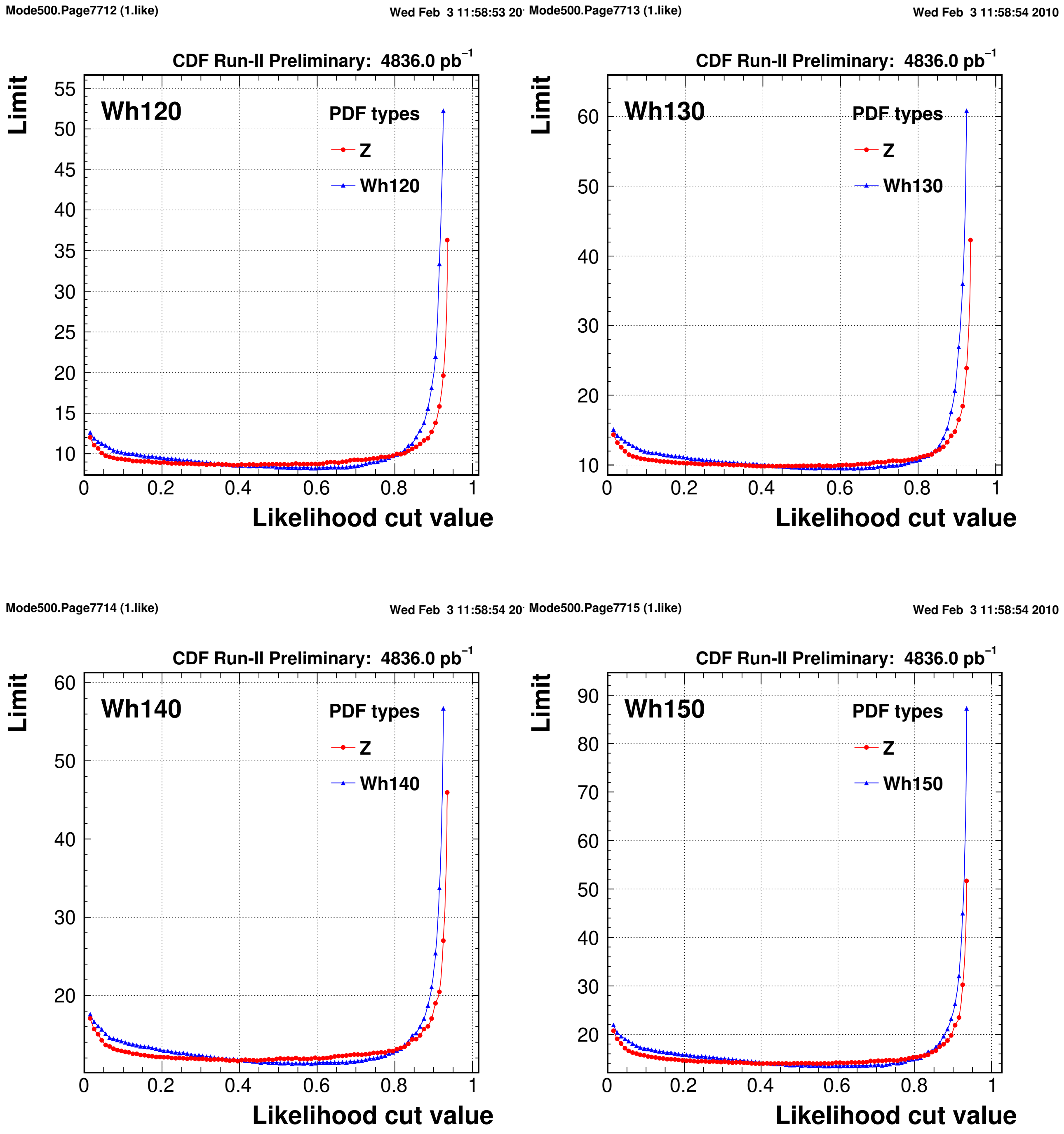

Figure 32: Limits as a function of CMX-likelihood cut-value for three types of signal PDFs and for different higgs masses. The background sample is the `Jet20`.

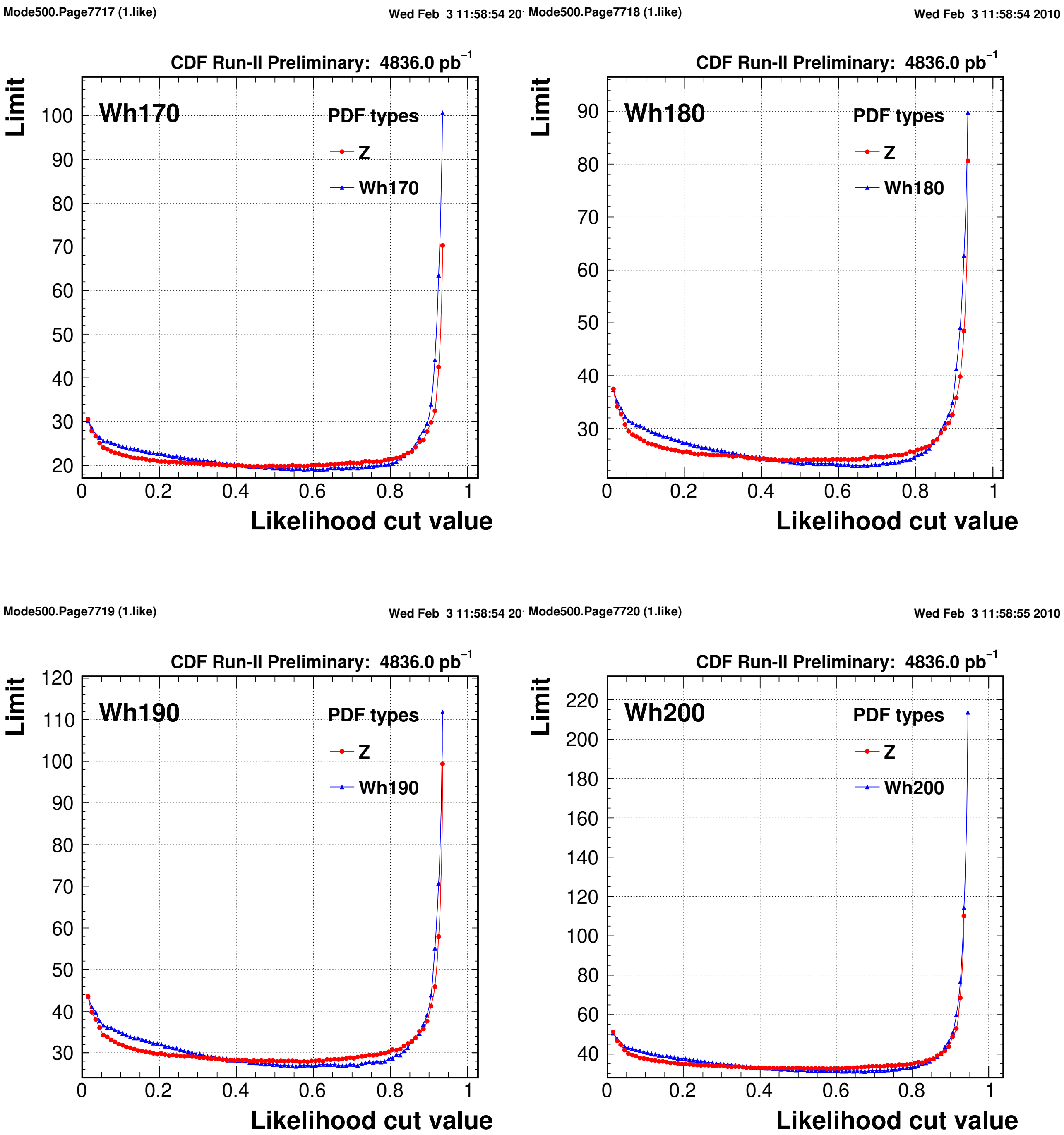

Figure 33: Limits as a function of CMX-likelihood cut-value for three types of signal PDFs and for different higgs masses. The background sample is the `Jet20`.

References

[1] V.Tiwari, G.Giurgiu, M.Paulini, J.Russ and B.Wicklund, "Likelihood Based Electron Tagging", CDF7121 (Version 1.3).

[2] Toru Okusawa, Yoshihiro Seiya, Takayuki Wakisaka, and Kazuhiro Yamamoto, "Baseline Selection of High-p_T Dilepton Events to Search for the Wh Production", CDF7260 (Version 3.0).

[3] Toru Okusawa, Yoshihiro Seiya, Takayuki Wakisaka, and Kazuhiro Yamamoto, "Search for the Wh Production Using High-p_T Like-Sign Dilepton Events in Run II", CDF7262 (Version 3.0).